

1 **Methane, ethane, and propane production in Greenland ice**
2 **core samples and a first isotopic characterization of excess**
3 **methane**

4 Michaela, Mühl¹, Jochen Schmitt¹, Barbara Seth¹, James E. Lee², Jon S. Edwards³, Edward J.
5 Brook³, Thomas Blunier⁴, Hubertus Fischer¹

6
7 ¹Climate and Environmental Physics and Oeschger Centre for Climate Change Research, University of Bern,
8 Bern, 3012, Switzerland

9 ²Los Alamos National Laboratory, Earth Systems Observation, Los Alamos, NM 87545, USA

10 ³College of Earth, Ocean, and Atmospheric Sciences, Oregon State University, Corvallis, OR 97331, USA

11 ⁴Centre for Ice and Climate, Niels Bohr Institute, University of Copenhagen, Copenhagen, 2200, Denmark

12

13 *Correspondence to:* Michaela Mühl (michaela.muehl@unibe.ch)

14

15

16

17

18

19

20

21

22

23

24

25

26

27

28

29

30

31

32

33

34

35

36 **Abstract.** Air trapped in polar ice provides unique records of the past atmospheric composition
37 ranging from key greenhouse gases such as methane (CH₄) to short-lived trace gases like ethane
38 (C₂H₆) and propane (C₃H₈). Recently, the comparison of CH₄ records obtained using different
39 extraction methods revealed disagreements in the CH₄ concentration for the last glacial in
40 Greenland ice. Elevated methane levels were detected in dust-rich ice core sections measured
41 discretely pointing to a process sensitive to the melt extraction technique. To shed light on the
42 underlying mechanism, we performed targeted experiments and analyzed samples for methane
43 and the short-chain alkanes ethane and propane covering the time interval from 12 to 42 kyears.
44 Here, we report our findings of these elevated alkane concentrations, which scale linearly with
45 the amount of mineral dust within the ice samples. The alkane production happens during the
46 melt extraction step of the classic wet extraction technique and reaches 14 to 91 ppb of CH₄
47 excess in dusty ice samples. We document for the first time a co-production of excess methane,
48 ethane, and propane, with the observed concentrations for ethane and propane exceeding their
49 past atmospheric background at least by a factor of 10. Independent of the produced amounts,
50 excess alkanes were produced in a fixed molar ratio of approximately 14:2:1, indicating a
51 shared origin. The measured carbon isotopic signature of excess methane is $(-47.0 \pm 2.9) \text{‰}$
52 and its deuterium isotopic signature is $(-326 \pm 57) \text{‰}$. With the co-production ratios of excess
53 alkanes and the isotopic composition of excess methane we established a fingerprint that allows
54 us to constrain potential formation processes. This fingerprint is not in line with a microbial
55 origin. Moreover, an adsorption-desorption process of thermogenic gas on dust particles
56 transported to Greenland appears not very likely. Instead, the alkane pattern appears to be
57 indicative of abiotic decomposition of organic matter as found in soils and plant leaves.

58

59 **1. Introduction**

60

61 Atmospheric air entrapped in polar ice represents a unique archive of the past atmospheric
62 composition including the concentration of greenhouse gases like carbon dioxide (CO₂),
63 methane (CH₄), and nitrous oxide (N₂O) but also short-lived trace gases such as ethane (C₂H₆)
64 and propane (C₃H₈). The ongoing anthropogenic increase in the atmospheric concentrations of
65 these gases makes a detailed understanding of their preindustrial variations and biogeochemical
66 cycling of paramount importance, and only polar ice cores are able to provide this information.
67 However, to interpret reconstructions of the atmospheric composition from polar ice cores
68 requires that archived atmospheric trace gases are not altered within the ice itself. Furthermore,
69 the air must be extracted from the ice sample without altering the original composition. Thus,

70 the comparison of ice core records obtained using different extraction techniques and from
71 different ice cores requires careful consideration and interpretation.

72

73 Not all drill sites or specific time intervals are equally suitable to derive pristine atmospheric
74 trace gas records. For example, CO₂ data from Greenland ice are subject to CO₂ in situ
75 production due to impurities in the ice (Anklin et al., 1995; Smith et al., 1997). In situ
76 production is also observed for N₂O, for example, in glacial Antarctic ice core samples
77 characterized by higher dust content (Schilt et al., 2010). In contrast, CH₄ in polar ice cores, in
78 the absence of melt layers, was considered to be not affected by in situ processes. However,
79 more recent results from Greenland ice showing elevated CH₄ concentrations in glacial dust-
80 rich ice (Lee et al., 2020) and high amplitude CH₄ spikes in Holocene ice (Rhodes et al., 2013,
81 2016) question this assumption.

82

83 This becomes especially worrisome as atmospheric methane shows a significant North-South
84 gradient, reflecting the predominance of Northern Hemisphere sources. Ice cores from
85 Greenland and Antarctica have been used to quantify this Inter-Polar Difference (IPD) in past
86 CH₄ concentrations (Chappellaz et al., 1997; Baumgartner et al., 2012, Beck et al., 2018) to
87 derive the relative contribution of Northern and Southern hemispheric sources to the overall
88 CH₄ changes. The Holocene IPD is on the order of several tens of ppb, i.e., one order of
89 magnitude smaller than the past atmospheric CH₄ concentration. Thus, any small CH₄ bias on
90 the order of a few ppb to tens of ppb strongly impacts the conclusions drawn from this IPD,
91 while the influence on the total radiative forcing by such small biases is negligible. In summary,
92 existing results of CH₄ concentrations from Greenland and Antarctic ice cores have to be
93 carefully scrutinized for such effects.

94

95 A first step in this direction has been made in previous work by Lee et al. (2020), for example
96 by comparing CH₄ records derived using different measurement techniques. Past CH₄
97 concentrations ([CH₄]) are retrieved by measurements of Greenland and Antarctic ice cores
98 using traditional discrete and relatively new continuous melt extraction techniques. While
99 discrete ice measurements deliver one single value for each sample, Continuous Flow Analysis
100 (CFA) gradually melts a thin stick of the ice core providing a continuous record for this section.
101 Although in both techniques the ice sample is melted, the CFA technique separates air from the
102 meltwater stream in about 1-2 min providing only a short time for any reaction in the water,
103 while for the discrete technique the contact time is typically 15-30 min. Comparing [CH₄]

104 histories from several Greenland ice cores measured discretely (NGRIP, GISP2, GRIP) with
105 the continuous Greenland NEEM and the continuous Antarctic WAIS records over the last
106 glacial period, higher [CH₄] can be found in the discrete Greenland measurements for specific
107 time intervals (Lee et al., 2020; Fig. 1 therein), where dust concentrations are especially high.

108
109 Looking at the NGRIP methane hydrogen isotope ($\delta\text{D-CH}_4$) record (Bock et al., 2010b), which
110 was also measured with a discrete melt extraction technique (Bock et al., 2010a), it turns out
111 that in the high dust ice sections, the isotopic values are also affected. Several negative $\delta\text{D-CH}_4$
112 excursions with a maximum depletion of 16 ‰ (permil) prior to the onset of Dansgaard-
113 Oeschger (DO) event 8 were identified (Bock et al., 2010b). At the time of that publication
114 there was no straightforward explanation for these $\delta\text{D-CH}_4$ depletions during times of a
115 relatively stable climate. Using ice from Antarctica, much smaller $\delta\text{D-CH}_4$ variations (3-4 ‰)
116 during this interval were found in measurements performed at the University of Bern
117 (unpublished data), again questioning the atmospheric origin of these $\delta\text{D-CH}_4$ depletions prior
118 to the DO onset.

119
120 All these observations in Greenland ice give reason to assume that a hitherto unknown process
121 exists that produces or releases additional methane in some time intervals in Greenland ice
122 cores (from here on referred to as “excess methane” or CH_{4(xs)}). This process is related to the
123 extraction technique (only found in records obtained by discrete melt extractions) and has only
124 been observed in glacial Greenland ice with high mineral dust concentrations.

125
126 A first attempt to characterize CH_{4(xs)} was made by Lee et al. (2020) who analyzed [CH₄] in
127 discrete ice samples with different impurity composition and concentration from several ice
128 cores (GISP2, NEEM, WAIS, SPICE) using a multiple melt-refreeze technique. They were able
129 to quantify CH_{4(xs)} contributions of up to 30-40 ppb for Greenland samples. Sequential melt-
130 refreeze extractions showed that the process leading to CH_{4(xs)} is slow and not completed during
131 the first melt-refreeze cycle (i.e., within around 30 min). A set of samples was analyzed with
132 the admixture of a HgCl₂ solution to suppress microbial activity in the meltwater. No difference
133 in the measured [CH₄] was observed between the poisoned samples and replicates without
134 HgCl₂, excluding a microbial CH₄ production after melting. In addition, Lee et al. (2020) used
135 the NGRIP [CH₄] (Baumgartner et al., 2014) and $\delta\text{D-CH}_4$ records (Bock et al., 2010b) to
136 estimate the deuterium isotopic signature of the CH_{4(xs)}. Assuming a two-component mixture

137 of atmospheric methane and excess methane, their model led to a best estimate of (-293 ± 31)
138 ‰ for δD - $CH_{4(xs)}$.

139
140 A straightforward explanation for $CH_{4(xs)}$ may be that CH_4 is either produced in the meltwater,
141 or it was produced beforehand and only released during the melt extraction. With respect to
142 that, Lee et al. (2020) reviewed several mechanisms that could account for the observed
143 variations in Greenland ice core records. None perfectly matched all their observations but
144 lastly, three of the proposed mechanisms were short-listed by Lee et al. (2020): (1) an
145 adsorption process on dust particles prior to the deposition on the ice sheet; (2) an in situ
146 production in the ice; or (3) an abiotic reaction during melt extraction.

147
148 Here we resume the work by Lee et al. (2020) and shed more light upon the potential formation
149 processes using a targeted and more comprehensive study to quantify $CH_{4(xs)}$. We analyzed
150 specific NGRIP and GRIP ice core samples discretely with two different wet extraction
151 systems. With our $\delta^{13}C$ - CH_4 device we are able to measure [methane], [ethane], [propane], and
152 $\delta^{13}C$ - CH_4 on a single ice sample in two subsequent extractions. With our second device we add
153 experimental information on δD - CH_4 . In Sect. 2, we provide information on our sampling
154 strategy and measurement techniques. With our new experimental results, presented in Sect. 3,
155 we provide quantitative data for $CH_{4(xs)}$ in NGRIP and GRIP samples and extend our
156 observations to other “excess alkanes” (ethane and propane), which are revealed to be co-
157 produced during the excess CH_4 production. The observed molar ratios between methane,
158 ethane, and propane are evaluated and their relation to the abundance of mineral dust (Ca^{2+})
159 within the ice samples is quantified. A 2nd extraction of the meltwater enables us to estimate
160 the temporal dynamics of excess alkane production. Using a Keeling-plot approach to our
161 isotopic results, we calculate the carbon and deuterium isotopic signature of excess CH_4 ($\delta^{13}C$ -
162 $CH_{4(xs)}$ and δD - $CH_{4(xs)}$). Based on our new and improved observations, we finally come back
163 to the discussion of the hypotheses proposed by Lee et al. (2020) in Sect. 4 and offer potential
164 mechanisms that could explain the excess alkanes in ice core samples. For readers not interested
165 in all the experimental details, we recommend to jump straight to Sect. 4 to see the discussion.

166
167
168

169 2. Ice core samples and measurements

170 2.1 Ice core samples

171

172 Mixing ratios of alkanes (methane, ethane, and propane) and the stable carbon ($\delta^{13}\text{C-CH}_4$) and
173 hydrogen ($\delta\text{D-CH}_4$) isotope ratios of methane were measured on ice core samples from the
174 North Greenland Ice Core Project (NGRIP) ice core. For this study, 19 NGRIP ice core samples
175 were measured for $\delta^{13}\text{C-CH}_4$ and alkane concentrations and nine NGRIP ice samples for $\delta\text{D-}$
176 CH_4 covering the depth between 1795.84 m and 1933.25 m. The NGRIP samples are from the
177 late glacial Marine Isotope Stages (MIS) 3 and 2 (22.6 to 30.6 kyears BP). These time intervals
178 are characterized by sharp atmospheric CH_4 increases in parallel to rapid warmings, the so-
179 called Dansgaard-Oeschger events, but we mostly sampled intervals with stable CH_4
180 concentrations. From the same time period, we also investigate measurements of 41 NGRIP
181 and 12 GRIP ice core samples which were carried out in 2011 and 2018, respectively, and
182 which have not previously been published. See Fig. 1 for an overview of all analyzed NGRIP
183 and GRIP ice core samples over time.

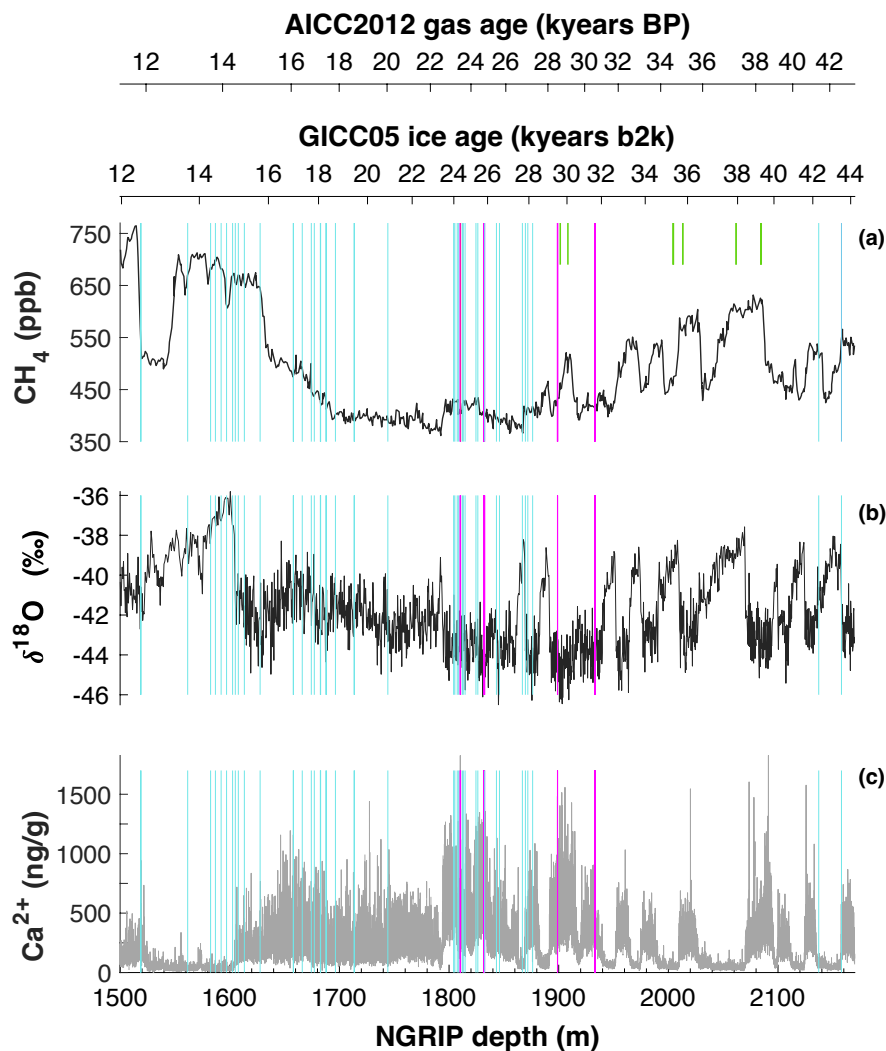
184

185 We also included 22 ice core samples from the European Project for Ice Coring in Antarctica
186 (EPICA) ice core from Dome C (MIS 4), which are not affected by a measurable excess CH_4
187 production and which we use as long-term monitoring ice for the system performance and to
188 quantify the blank contribution of the analytical system (see Appendix B).

189 The late glacial period, which includes the age of most of the measured NGRIP samples, is
190 characterized by an overall high impurity and dust content and low atmospheric methane
191 concentrations. For our analysis, we have selected ice core bags (where for NGRIP and GRIP
192 ice cores, a bag is a 55 cm long ice core section) in which we expect the same atmospheric CH_4
193 concentration but see a high range of mineral dust content (Ca^{2+}). In this way, we can compare
194 neighbouring samples with the same low stadial CH_4 levels due to stable atmospheric
195 concentrations and temporal smoothing by the slow bubble enclosure process but are expected
196 to vary in measured concentrations due to contributions of excess alkanes. Ca^{2+} content across
197 our NGRIP samples ranges from 307 ng/g to 1311 ng/g. This sample selection is critical to
198 quantify the isotope signature of the $\text{CH}_{4(\text{xs})}$ produced using the Keeling-plot approach (Keeling,
199 1958). The underlying assumptions of this mass balance approach are (1) that there is only a
200 two-component mixture (atmospheric methane and excess methane) and (2) that the isotopic
201 ratio of the mixture changes only by a varying input of the second source ($\text{CH}_{4(\text{xs})}$).

202

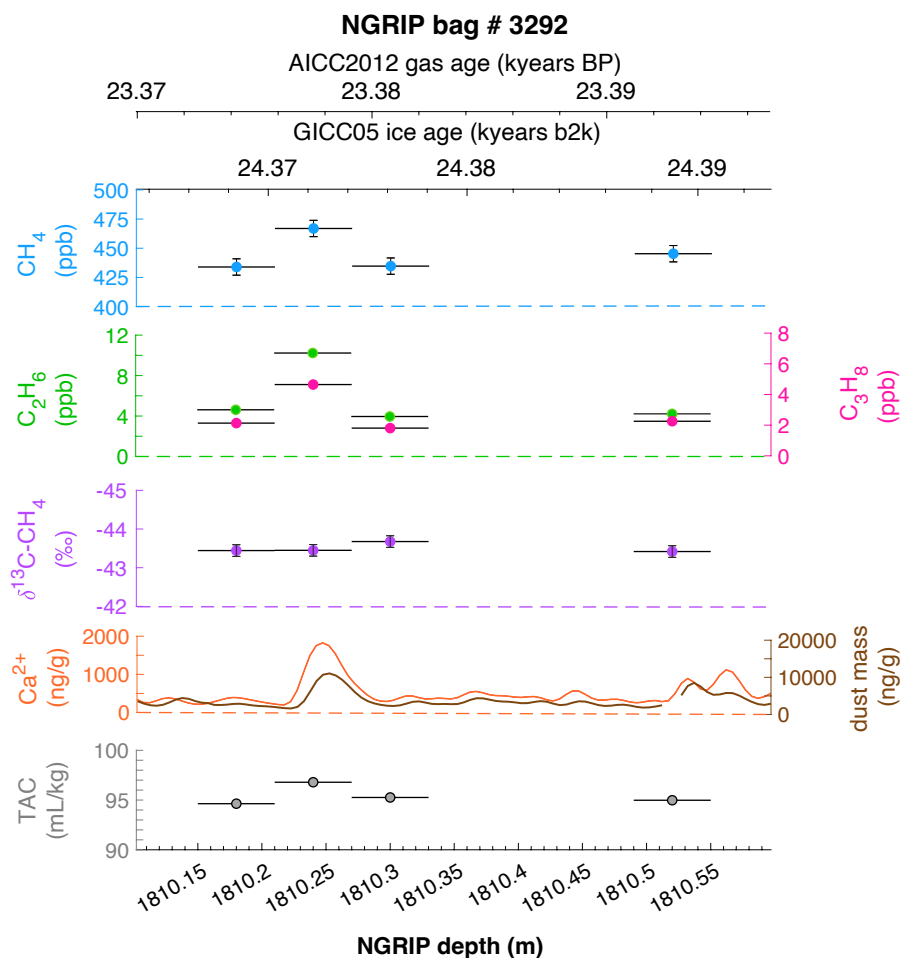
203 To select the samples, we use high-resolution mineral dust records measured using an Abakus
 204 laser attenuation device (Klotz, Germany) for particulate dust (Ruth et al., 2003) as well as Ca^{2+}
 205 concentrations (Erhardt et al., 2022) as dissolved mineral dust tracer derived from the Bern
 206 Continuous Flow Analysis System (Kaufmann et al., 2008). In principle, particulate dust and
 207 the soluble dust tracer Ca^{2+} are strongly correlated. However, depending on acidity of the ice
 208 (mainly due to H_2SO_4 and HNO_3), variable amounts of CaCO_3 are converted into soluble CaSO_4
 209 and $\text{Ca}(\text{NO}_3)_2$, leading to a variable $\text{Ca}^{2+}/\text{dust}$ ratio (Legrand and Delmas, 1988). As an
 210 example, Fig. 2 shows the Ca^{2+} and mineral dust concentration of the NGRIP bag 3292 which
 211 we used to select the individual samples and the relevant parameters measured for each sample
 212 of this bag. The data overview for all other measured NGRIP bags can be found in Appendix
 213 A.



214
 215 **Figure 1: Overview of the analyzed NGRIP and GRIP samples over time.** All analyzed NGRIP and GRIP ice
 216 core samples are indicated on the NGRIP depth (m) on the bottom axis. To indicate an age for the gas and ice
 217 records both the AICC2012 gas age (kyears BP) and the GICC05 ice age (kyears b2k) scale are provided on the
 218 upper axes. Note that for the purpose of describing the excess CH_4 production in a certain ice sample the age is
 219 not important and we provide all records on depths throughout this manuscript. NGRIP samples measured from

220 the five main bags (3292, 3331 & 3332, 3453, 3515) for the Keeling-plot approach are indicated with vertical lines
 221 in pink, NGRIP samples measured in 2011 and individual NGRIP ice core samples measured in 2019-2020 (not
 222 included in the Keeling-plot analyses) in turquoise, and GRIP ice core samples in green. (a) [CH₄] record measured
 223 by wet extraction from NGRIP samples from Baumgartner et al. (2012, 2014). (b) δ¹⁸O record from North
 224 Greenland Ice Core Project members (2004). (c) Ca²⁺ record from Erhardt et al. (2022).

225



226
 227 **Figure 2: Detailed data overview for NGRIP bag 3292.** Bag-specific overview of several parameters measured
 228 for each sample in this bag at a given depth: methane, ethane, propane, Ca²⁺, mineral dust mass, TAC (Total Air
 229 Content), δ¹³C-CH₄. At the top the AICC2012 gas age (upper top axis) and the GICC05 ice age (lower top axis) of
 230 the respective depth are indicated. The mineral dust record is taken from Ruth et al. (2003), the Ca²⁺ record from
 231 Erhardt et al. (2022). The data overview for all further measured NGRIP bags can be found in Appendix A.

232

233

234 2.2 CH₄, C₂H₆, C₃H₈ and δ¹³C-CH₄ Analysis of Ice Core Samples

235

236 The short-chain alkanes and δ¹³C-CH₄ were measured at the University of Bern using the
 237 discrete wet extraction technique described in Schmitt et al. (2014). With this method, it is
 238 possible to measure mixing ratios of methane, ethane, and propane as well as the methane
 239 carbon isotopic signature and other trace gases on a single ice core sample of about 150 g.

240

241 Briefly, ice core samples are placed in a glass vessel locked by a stainless-steel flange which is
 242 attached to the vacuum line to evacuate laboratory air (see Fig. 3, step a). Before melting the

243 ice sample, the leak tightness of the vacuum extraction line is tested with a so-called He blank.
244 The ice sample is then melted under vacuum with the help of infrared radiation for ~35 min to
245 release the enclosed air (step b). The released air is continuously removed from the sample
246 vessel by a pressure gradient towards an adsorbing AirTrap (activated carbon), collecting all
247 relevant air components at -180°C. After melting is completed, the temperature of the meltwater
248 is stabilized close to 0°C, but does not refreeze again. Afterwards, He is sparged with 4 mL/min
249 at standard temperature and pressure (equivalent to 100-400 mL at the varying low pressure in
250 the headspace) through the melt water for ~14 min through a capillary at the bottom of the
251 vessel to transfer any remnant gas species dissolved in the melt water onto the AirTrap (step c).
252 The sample vessel is then isolated by closing the inlet and outlet valves (step d). Consecutively,
253 the AirTrap is warmed up in two steps to first remove N₂ and O₂ and in a second step to release
254 the gases of interest which are then sent after a cryofocus step to the gas chromatograph (GC)
255 for separation and quantification using an isotope ratio mass spectrometer (Isoprime 100,
256 Elementar).

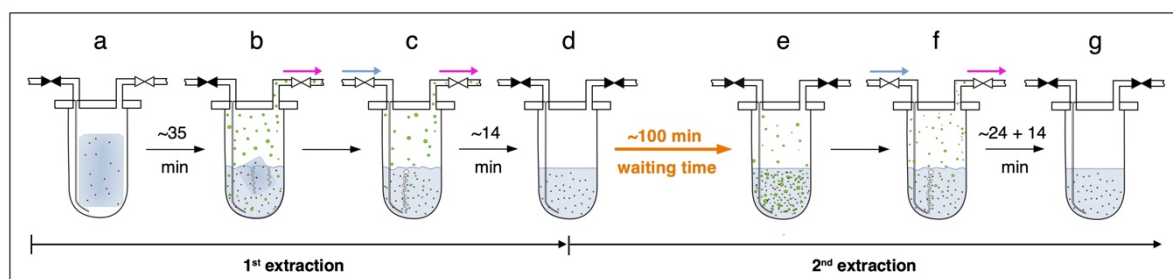
257
258 Precision of this method for CH₄ is about 8 ppb and 0.1 ‰ for δ¹³C-CH₄ based on the
259 reproducibility of the 1st extraction of ice core samples where isotopic data are expressed using
260 the δ notation on the international Vienna Pee Dee Belemnite (VPDB) scale. For C₂H₆, the
261 precision is 0.02 ppb or 1 ‰, for C₃H₈, 0.03 ppb or 5 ‰ (whatever is higher) based on the
262 reproducibility of standard air samples which are by definition not subject to excess production
263 (Schmitt et al., 2014). Blank levels for these species based on melted artificial (gas-free) ice
264 samples are 1-2 ppb for CH₄, 0.3 ppb for C₂H₆ and 0.2 ppb for C₃H₈ (Schmitt et al., 2014),
265 which are below the values measured on Antarctic ice, where excess production is minimal
266 compared to glacial Greenland samples (see Appendix B for details).

267
268 With their experimental investigations, Lee et al. (2020) were already able to demonstrate that
269 production/ release of CH_{4(xs)} is time-dependent. We therefore conclude that this process does
270 not have to be completed in the time available for the gas extraction described above. We
271 continued the analyses of excess alkane production with an additional extraction step (here
272 referred to as 2nd extraction, steps d-g in Fig. 3) following the normal ice extraction routine.
273 After all sample air is collected in the 1st extraction, the meltwater is left in the isolated sample
274 vessel (the vessel is closed and not connected to the carbon trap) and held at temperatures close
275 to 0°C for ~100 min (step d). After this “waiting time” of ~100 min, He is purged through the
276 meltwater for ~24 min to extract the gases that have been accumulated during this time interval

277 simulating the extraction time of the 1st extraction, followed by another ~14 min of He purging
 278 to mimic the last step of the ice extraction when the sample had completely melted (step f). The
 279 gases from this 2nd extraction are collected and measured following the same trapping and
 280 separation steps as in the 1st extraction. Note that the procedure of the 2nd extraction can be
 281 repeated any number of times (e.g. 3rd extraction).

282
 283 The amount of gases that we obtain from the 1st extraction comprises the atmospheric amount,
 284 a possible contribution by in situ production, and a potential time-dependent production/release
 285 in the meltwater (*in extractu*). The 2nd extraction, however, targets only the *in extractu* fraction.
 286 The system blank for the 2nd extraction was estimated using the 2nd extraction of Antarctic ice
 287 (Talos Dome, EDC) and were 2 ppb, 0.3 ppb and 0.3 ppb for CH₄, C₂H₆ and C₃H₈, respectively,
 288 assuming an ice core sample air volume of 14 mL at standard temperature and pressure, which
 289 is the typical ice sample size of 150 g with a total air content of 0.09 mL/g. For CH₄ this is <
 290 1% of the amount of extracted species in the 1st extraction of glacial Greenland ice. Due to the
 291 small amount of CH₄ analyzed in this 2nd extraction (about a factor of 20 to 50 less than for an
 292 ice core sample) the precision for the $\delta^{13}\text{C}$ analysis is much lower than for the 1st (ice sample)
 293 extraction and we estimate the precision of $\delta^{13}\text{C}$ -CH₄ to 2 ‰ and for [CH₄] to be 2 ppb or 10
 294 ‰ (based on the reproducibility of 2nd extractions of Antarctic EDC samples). For C₂H₆ and
 295 C₃H₈, the precision is comparable to the 1st extraction. Note that throughout the manuscript we
 296 do not perform blank corrections (neither for the measured alkane concentrations nor for the
 297 isotopic values). The only exception is for the calculation of the temporal dynamics of excess
 298 ethane production (see Appendix C) as the blank contribution would otherwise bias the samples
 299 with low Ca²⁺ content.

300
 301



302
 303 **Figure 3: Sequential steps (a-g) happening in the ice core sample vessel during the 1st and the 2nd extraction**
 304 **in the $\delta^{13}\text{C}$ -CH₄ extraction line.** Scheme illustrates the subsequent steps as described in detail in the text.
 305 Brownish spots indicate dust particles in the ice/ meltwater. Green circles indicate gas species (methane, ethane,
 306 and propane) in the meltwater or in the headspace of the vessel. Closed valves are indicated in black, open valves
 307 in white. Blue arrows indicate the He flow through the inlet capillary into the sample vessel, pink arrows indicate
 308 the flow direction from the sample vessel towards the AirTrap.

309 **2.3 $\delta\text{D-CH}_4$ Analysis of Ice Core Samples**

310
311 All $\delta\text{D-CH}_4$ data presented here were measured at the University of Bern using the discrete wet
312 extraction technique described in Bock et al. (2010a, 2014). This $\delta\text{D-CH}_4$ device allows to
313 measure the concentration of methane and its deuterium isotopic signature ($\delta\text{D-CH}_4$) on a single
314 ice core sample of about 300 g.

315
316 Briefly, ice core samples are melted after evacuation of the headspace using a warm water bath
317 at 40°C for 25-30 min to release the enclosed air into the sample vessel headspace. Once all the
318 ice is melted, the warm water bath is replaced by an ice-water bath to keep the meltwater
319 temperature and water vapor pressure low but without refreezing. In contrast to the $\delta^{13}\text{C-CH}_4$
320 method, the inlet and outlet valves are closed during the melting process. The released air leads
321 to an increased pressure in the sample vessel headspace enhancing the solubility of gases in
322 water. After the melting is complete, the inlet and outlet valves are opened and He is purged
323 for ~40 min with a flow of 360 mL/min to transfer the accumulated air in the headspace and
324 bubble He through the meltwater to strip dissolved gases. Just like for the $\delta^{13}\text{C-CH}_4$ method,
325 the air is collected on an activated carbon trap followed by further purification steps including
326 GC separation. Note that compared to the $\delta^{13}\text{C-CH}_4$ device, we performed only one extraction
327 with the $\delta\text{D-CH}_4$ device.

328
329 For both methods, we assume that the time for an *in extractu* production during the ice
330 extraction procedure starts with the first presence of meltwater until He purging is stopped.
331 Note that this time is considerably longer for the $\delta\text{D-CH}_4$ analysis (~60 min) compared to the
332 time of the 1st extraction in the $\delta^{13}\text{C-CH}_4$ analysis (~35 min).

333
334 Using this method we can measure $[\text{CH}_4]$ and $\delta\text{D-CH}_4$ with a precision of about 15 ppb and 3
335 ‰ (based on standard ice sample measurements), where isotopic data are expressed using the
336 δ notation on the international Standard Mean Ocean Water (SMOW) scale.

337

338 **3. Characterization of excess alkanes in ice cores**

339 **3.1 Methane, ethane, propane concentrations**

340

341 As described in detail in Sect. 2.2 a full ice sample measurement includes the regular ice sample
342 extraction (1st extraction) and, after the waiting time of ~100 min, a 2nd gas extraction in the
343 meltwater. Gas from the 1st extraction comprises atmospheric air, a possible contribution from

344 in situ production, a potential time-dependent contribution by an *in extractu* process, and any
345 contribution from the device itself (blank). For the gas species discussed here (methane, ethane,
346 propane), these individual fractions are very different in magnitude. For polar ice core samples,
347 the atmospheric air is the major fraction of methane even in dust-rich, glacial ice from
348 Greenland prone to CH_{4(xs)} production (see below). The opposite is expected for ethane and
349 propane, which are dominated by the *in extractu* component in dust-rich Greenland ice. To
350 establish a better knowledge of alkanes in Greenland ice, we evaluated the measured
351 concentrations of methane, ethane, and propane, their ratios to each other and the relation to the
352 content of mineral dust in the ice for both the 1st and the 2nd extraction.

353

354 Note that different units to indicate concentrations of the trace gases of interest are used
355 throughout this study. By using mixing ratios in units of [ppb], as typically used for atmospheric
356 concentrations, the concentration of trace gases is related to the amount of air extracted from
357 the ice. Ice core samples with a low air content cause higher mixing ratio values for any
358 additional molecules produced in situ or *in extractu* compared to ice core samples with a high
359 air content and the interpretation might be biased. Alternatively, for any additional molecules
360 produced in situ or *in extractu*, [mol absolute per sample] denotes the absolute amount of trace
361 gases and is independent of the ice core air content. In the following, both units are used and
362 great care has to be taken to avoid misinterpretation of the results with respect to the different
363 units.

364

365 **3.1.1 Excess alkanes in the 1st extraction**

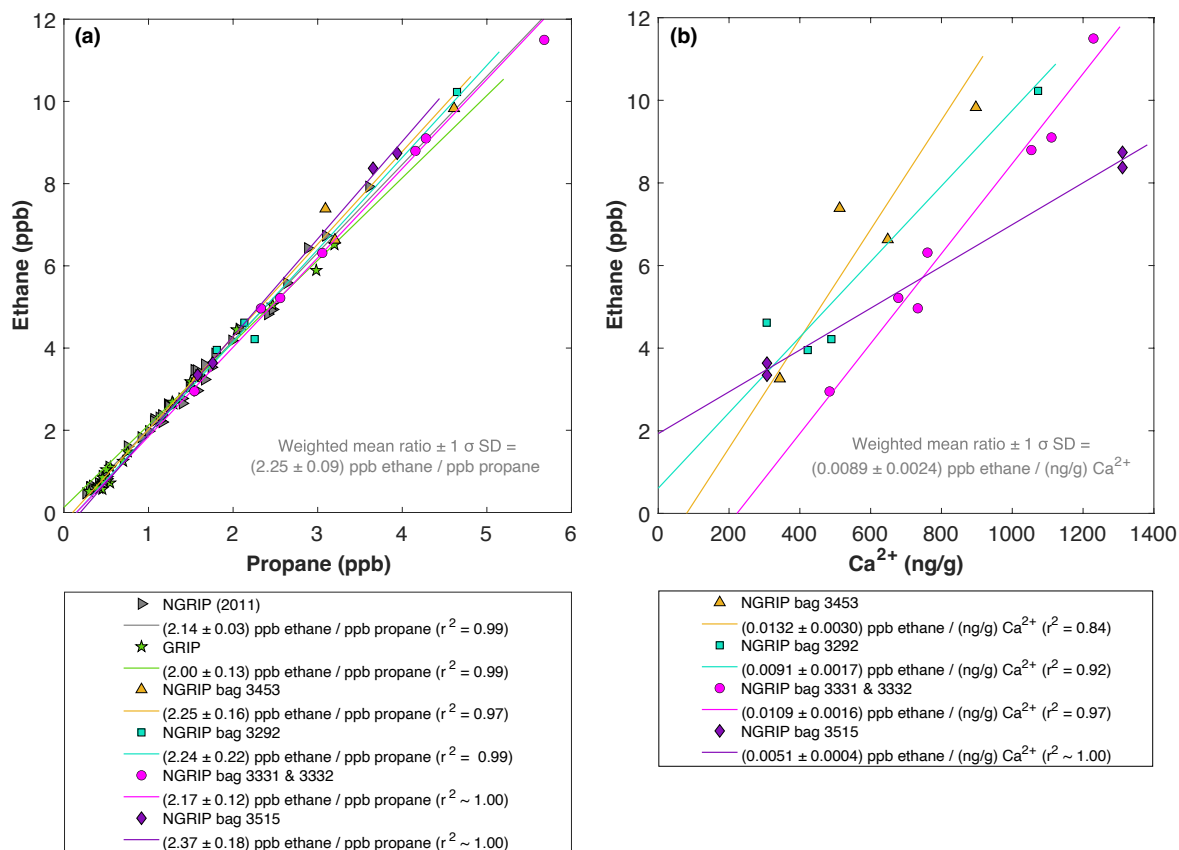
366

367 Figure 4 and 5 show results from the 1st extraction of our NGRIP and GRIP ice core samples.
368 For dust-rich samples, ethane ranges between 2 ppb and 12 ppb, and propane concentrations
369 between 1 ppb and 5 ppb. In contrast, low-dust samples from both GRIP and NGRIP have much
370 lower concentration (ca. 0.5 ppb for ethane, and 0.3 ppb for propane) consistent with estimates
371 of past atmospheric ethane and propane concentrations from the 15th to 19th century of the
372 common era being about 0.4 ppb in Greenland ice (Nicewonger et al., 2016) and lower for
373 propane (Helmig et al., 2013). Emissions of ethane and propane were likely reduced during the
374 glacial (Bock et al., 2017; Nicewonger et al., 2016; Dyonisius et al., 2020) thus, 0.5 ppb appears
375 to be an upper limit of past atmospheric concentrations of ethane and propane. This estimate of
376 past atmospheric ethane concentrations is an order of magnitude smaller than the values we
377 obtained from our dust-rich ice core samples from the 1st extraction, pointing to a strong

378 additional source of these alkanes for dust-rich samples. Thus, the unusually high mixing ratios
379 indicate that ethane and propane in glacial ice extracted using our melt technique on discrete
380 samples do not represent atmospheric levels.

381

382 As illustrated in Fig. 4 (left panel), the ethane and propane concentrations are highly correlated,
383 pointing to a common production of excess ethane and excess propane. The weighted mean
384 ratio and its weighted standard deviation (both weighted according to the number of samples
385 measured per bag) is (2.25 ± 0.09) ppb ethane/ ppb propane. Note that all regression lines are
386 calculated by following the method of York (1968) and York et al. (2004). York's analytical
387 solution to the best-fit line accounting for normally distributed errors both in x and y is widely
388 used to determine an isotopic mixing line and has been proven as the least biased method (Wehr
389 and Saleska, 2017; Hoheisel et al., 2019). Throughout the manuscript we use the 1 sigma (1σ)
390 standard deviation to express uncertainties. In Fig. 4, where the individual bags studied are
391 color-coded, we can clearly see that the ratio is essentially the same between the individual bags
392 and that the correlation is also very high within each bag (although we have to consider for the
393 significance of this correlation that the number of samples per bag is very low). This indicates
394 that for NGRIP ice ethane and propane are found in a fixed ratio. Accordingly, excess ethane
395 and propane production can be well represented by the weighted mean ratio and ethane and
396 propane are produced in a ratio of approximately 2:1. Very similar results were also observed
397 in NGRIP samples measured in 2011 and in GRIP samples revealing an ethane to propane ratio
398 of 2.14 ± 0.03 ($r^2 = 0.99$) and 2.00 ± 0.13 ($r^2 = 0.99$), respectively (see Fig. 4, left panel).



399

400 **Figure 4: NGRIP and GRIP results of ethane and propane from the 1st extraction.** (a) Concentrations of
 401 ethane and propane and their ratios to each other for NGRIP and GRIP samples measured in the 1st extraction of
 402 the $\delta^{13}\text{C}$ - CH_4 device. Colors and symbols indicate the different NGRIP bags or cores used. (b) Bag-specific
 403 production ratios of ethane in relation to the Ca^{2+} concentration for NGRIP samples. Note that for bag 3515 there
 404 is a data gap in the Ca^{2+} record and an anomaly of the Ca^{2+} to dust mass ratio for the replicate sample at 1932.7 m.
 405 Thus, the Ca^{2+} concentration for these two data points is likely overestimated (see Fig. A3).

406

407

408 Methane concentrations range from 407 ppb to 476 ppb and are predominantly of atmospheric
 409 origin (see Fig. 5). The amount of $\text{CH}_{4(\text{xs})}$ is the difference between the measured methane
 410 concentration and the atmospheric background concentration. To quantify $\text{CH}_{4(\text{xs})}$ we use the
 411 fact that due to the low-pass filtering of the bubble enclosure process all samples within one
 412 bag should have the same atmospheric CH_4 concentration. This also ensures that any physical
 413 processes that potentially influence the atmospheric alkanes in our samples (gravitational
 414 enrichment, thermodiffusion, disequilibrium effects on CH_4 isotopes) are the same for all
 415 samples within one bag. The only difference between these samples is, thus, the degree of
 416 $\text{CH}_{4(\text{xs})}$ production which can be estimated from the linear fit between the measured CH_4
 417 concentration and the concentration of another species (e.g. ethane, propane, mineral dust, or
 418 Ca^{2+}), which serves as a proxy for $\text{CH}_{4(\text{xs})}$ production. The closest relationship was found for
 419 $[\text{C}_2\text{H}_6]$ and quantifying $\text{CH}_{4(\text{xs})}$ was done by extrapolating the linear regression between ethane

420 and methane to an ethane concentration of 0.39 ppb, the assumed atmospheric [C₂H₆]. This
421 leads to an estimate of the true atmospheric [CH₄] value within the respective bag, a value that
422 can then be subtracted from the measured CH₄ concentration to obtain the CH_{4(x_s)} in each
423 sample. The uncertainty of the calculated CH_{4(x_s)} is typically 8 ppb.

424

425 Using the relation of ethane to methane this approach translates into CH_{4(x_s)} in the range of 14
426 ppb to 91 ppb for these five NGRIP bags with a mean excess of 39 ppb. Equivalent calculations
427 can be made using propane, dust, or Ca²⁺ as proxy for CH_{4(x_s)} production, however, the
428 relationship between dust parameters and CH_{4(x_s)} is more variable and does not lead to equally
429 precise values for CH_{4(x_s)}. Nevertheless, the obtained mean CH_{4(x_s)} using the relation of mineral
430 dust or Ca²⁺ to methane is similar in size to the one obtained by ethane.

431

432 We find a constant production ratio between all three excess alkanes for all bags investigated.
433 The weighted mean production ratio and its weighted standard deviation was calculated to be
434 (6.42 ± 1.57) ppb methane / ppb ethane and (14.3 ± 3.7) ppb methane/ ppb propane for the
435 samples of the five main NGRIP bags, and (2.25 ± 0.09) ppb ethane/ ppb propane (also
436 including NGRIP2011 and GRIP here). Note that there is a flagged sample for CH₄ in bag 3453
437 (yellow asterisk in Fig. 5), where one vent (V6) was unintentionally open during the
438 measurement, which may have compromised the result. We therefore excluded the production
439 ratio determined from bag 3453.

440

441 In summary, we can characterize the excess alkane production in our measured NGRIP samples
442 by an overall methane/ethane/propane ratio of approximately 14:2:1. This constant relationship
443 between different alkanes suggests that excess alkanes are produced in a fixed ratio by a
444 common production process.

445

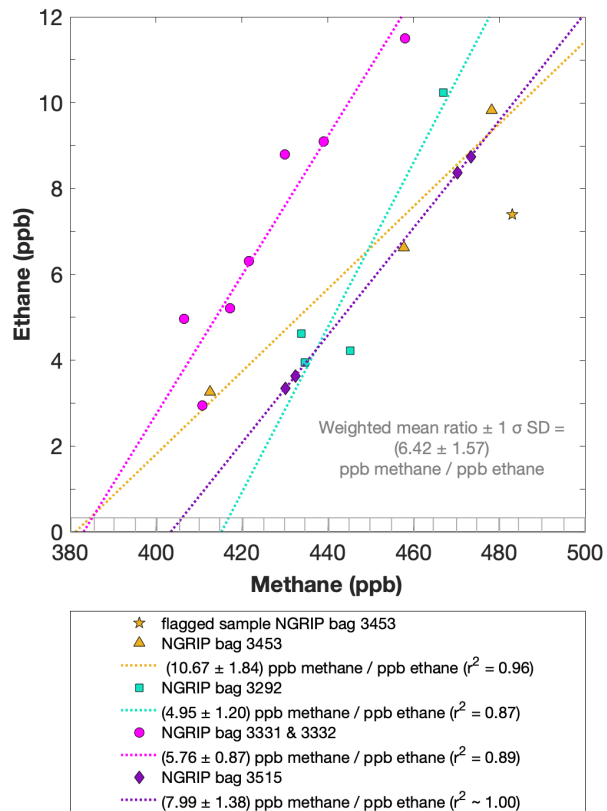
446 Another important observation is the close relation between excess alkanes and the content of
447 mineral dust within the ice core samples. Using measurements on GISP2 and NEEM ice core
448 samples, Lee et al. (2020) reported for the first time the close relation of CH_{4(x_s)} to chemical
449 impurities with the highest correlation with Ca²⁺. This is supported by our measurements on
450 NGRIP and GRIP samples revealing an overall increase of CH_{4(x_s)}, ethane, and propane with
451 increasing Ca²⁺ (see for example the ethane/Ca²⁺ relationship in Fig. 4, right panel). Although
452 the connection between ethane and Ca²⁺ is more variable than for ethane and propane between
453 the different bags, the slopes of the linear regressions in Fig. 4 (right panel) are still the same

454 within the 2σ uncertainty and the weighted mean ratio of all NGRIP samples amounts to
 455 (0.0089 ± 0.0024) ppb ethane/ (ng/g) Ca^{2+} . However, this weighted mean value is likely biased
 456 low due to the relatively low ethane/ Ca^{2+} slope of bag 3515. Due to a data gap at 1932.7 m in
 457 the Ca^{2+} record, the corresponding Ca^{2+} concentration for two of the samples of this bag is
 458 subject to a large interpolation error and overestimated Ca^{2+} (see Fig. A3).

459
 460 The results agree with results from GRIP and earlier NGRIP (2011) measurements, revealing
 461 an ethane/ Ca^{2+} ratio of 0.0105 ± 0.0029 ($r^2 = 0.76$) and 0.0090 ± 0.0006 ($r^2 = 0.91$),
 462 respectively.

463 Based on the fixed ratio of $\text{CH}_{4(\text{xs})}$ and ethane described above this translates into a weighted
 464 mean excess $\text{CH}_4/\text{Ca}^{2+}$ ratio of (0.0529 ± 0.0111) ppb methane per (ng/g) Ca^{2+} .

465



466
 467 **Figure 5: NGRIP results of methane and ethane from the 1st extraction.** Concentrations of methane (ppb) and
 468 ethane (ppb) and their ratios to each other for NGRIP samples measured in the 1st extraction of the $\delta^{13}\text{C}\text{-CH}_4$
 469 device. Different colors and symbols indicate the different NGRIP bags used for our analysis. Note that there is a
 470 flagged sample for CH_4 in bag 3453 as indicated with a yellow asterisk, which is not included in the ratio of bag
 471 3453. The grey hatched area indicates past atmospheric ethane concentrations of maximum 0.39 ppb as estimated
 472 by Nicewonger et al. (2016).

473

474

475

476 3.1.2 Excess alkanes in the 2nd extraction

477

478 With the 2nd extraction of the $\delta^{13}\text{C}\text{-CH}_4$ analyses we can evaluate the temporal dynamics of
479 excess alkane production, assuming that all alkanes extracted in the 2nd extraction were
480 produced after the 1st extraction was completed.

481 For our Greenland samples we measured a range of about 0.2 to 2.4 pmol for ethane and a range
482 of 0.1 to 1.2 pmol for propane in the 2nd extraction (Fig. 6, right panel). These values in pmol
483 are equivalent to 0.2 to 4.8 ppb of ethane and 0.2 to 2 ppb of propane assuming that the amount
484 of excess alkanes was added to 14 mL of ice core air (which is the typical ice sample size of
485 150 g with a total air content of 0.09 mL/g). The measured amount of methane ranges between
486 3 pmol and 20 pmol (Fig. 6, left panel).

487

488 The ratio of the measured amount for the individual species between the 1st and the 2nd
489 extraction amounts to 3.6 ± 0.85 ($r^2 = 0.78$) for ethane (Fig. 7, right panel), 3.3 ± 0.33 ($r^2 =$
490 0.78) for propane (combined data of NGRIP and GRIP) and 3.8 ± 1.62 ($r^2 = 0.33$) for methane
491 (only NGRIP data), where the uncertainty for CH_4 is again much larger. Thus, we can conclude
492 that the amount of alkanes produced during the waiting time after the 1st extraction until the 2nd
493 extraction was finished, was approximately 30% of the amount produced during the 1st
494 extraction. Results from the 2nd extraction also demonstrate that this process is slow and not
495 completed during the 1st extraction. We can thereby confirm the results of Lee et al. (2020) but
496 we are able to show for the first time that this process leads also to production of excess ethane
497 and propane.

498

499 For a better estimate of the temporal reaction kinetics of the underlying process, we can relate
500 the measured amount of the individual species to the time available for a potential reaction in
501 the meltwater during each extraction. For the five GRIP samples that were measured with a 2nd
502 and 3rd extraction (see Sec. 2.2 for details) we take the cumulative production amount (where
503 the first data point is the produced amount in the 1st extraction, the second data point is the sum
504 of the 1st and 2nd extraction, and the third data point is the sum of the 1st, 2nd, and 3rd extraction).
505 In the example shown for ethane (Fig. C1, Appendix C), we can see the assumed first-order
506 reaction kinetics with a decreasing ethane accumulation over time providing a good model for
507 our measurements (details on the calculation can be found in Appendix C). With that, we can
508 estimate the half-life time (τ) of the production to be approximately 30 min. Note that this long
509 half life has also an implication for a potential excess production of CH_4 in continuous flow

510 techniques, where the time before the air is separated from the liquid water stream is only 1-2
511 min. Thus, only 5-10 % of the *in extractu* production found in our 1st extraction can be expected
512 in such continuous flow techniques, which are difficult to detect.

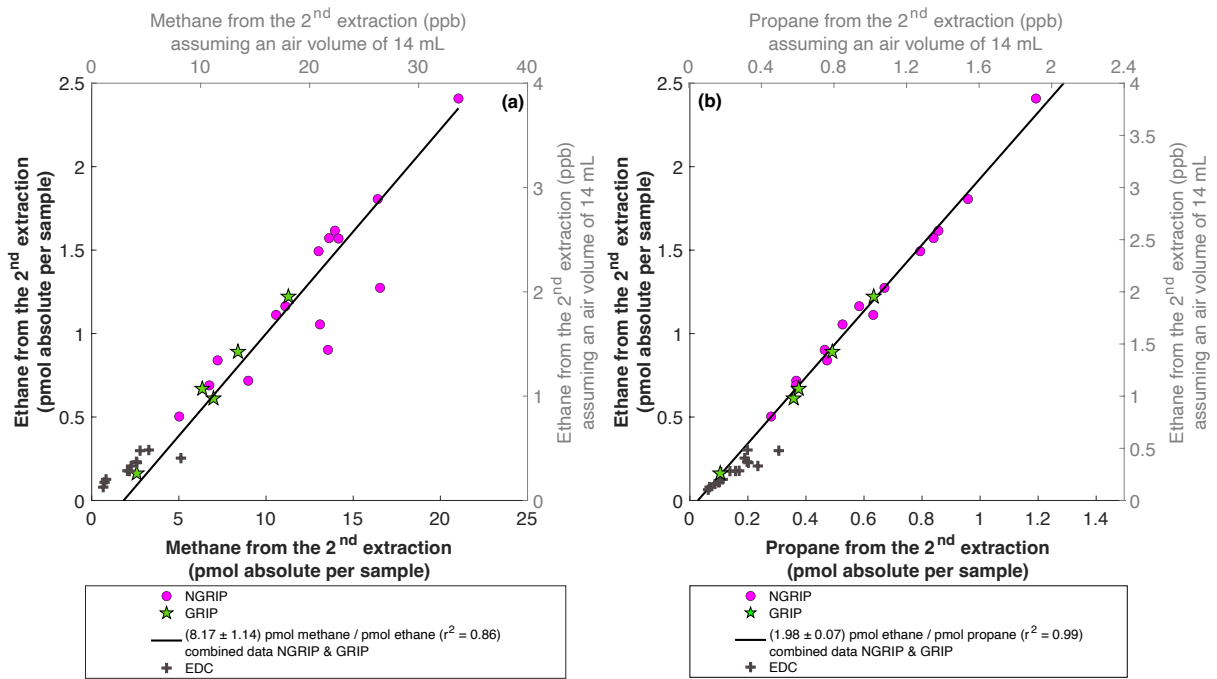
513
514 The goodness of fit of the ratios of the measured concentrations between the 1st and the 2nd
515 extraction is $r^2 = 0.78$ for both ethane and propane, indicating that the production/release in the
516 1st extraction in relation to the 2nd extraction is well correlated for both species (see Fig. 7b for
517 ethane). Thus, samples that produced higher excess alkanes during the 1st extraction also
518 produced more excess alkanes in the 2nd extraction, suggesting that the production is dependent
519 on the amount of some reactant present in the samples from which excess alkanes are produced.
520 Again, for CH₄ this relationship is more variable which is likely related to the higher uncertainty
521 in measuring CH₄ for the 2nd extraction.

522
523 The ratio of ethane to propane of all measured Greenland samples in the 2nd extraction is 1.98
524 ± 0.07 ($r^2 = 0.99$). The ratio of methane to ethane is 8.17 ± 1.14 ($r^2 = 0.86$). Accordingly, the
525 overall relationship between methane, ethane, and propane in the 2nd extraction can be
526 characterized by a ratio of approximately 16:2:1. However, comparing the ratios of
527 ethane/propane and methane/ethane between the 1st and the 2nd extraction, there is no significant
528 difference within the 2σ uncertainties from 2.25 ± 0.09 to 1.98 ± 0.07 , and from 6.42 ± 1.57 to
529 8.17 ± 1.14 . We can conclude that within the error limits, the production ratios stayed the same,
530 suggesting that the same *in extractu* process is at play during both extractions.

531
532 In the 2nd extraction, we can again observe the relation between excess alkanes and the amount
533 of mineral dust. Figure 7a shows the correlation of ethane (fmol/g meltwater) to Ca²⁺ (ng/g) in
534 all measured NGRIP and GRIP samples in the 2nd extraction revealing a production of $(0.0085$
535 $\pm 0.0011)$ fmol/(g meltwater) ethane per (ng/g) Ca²⁺ with $r^2 = 0.70$. For methane, we observe a
536 production ratio of (0.0556 ± 0.01513) fmol/(g meltwater) methane per (ng/g) Ca²⁺ with a
537 correlation of $r^2 = 0.47$ (data not shown).

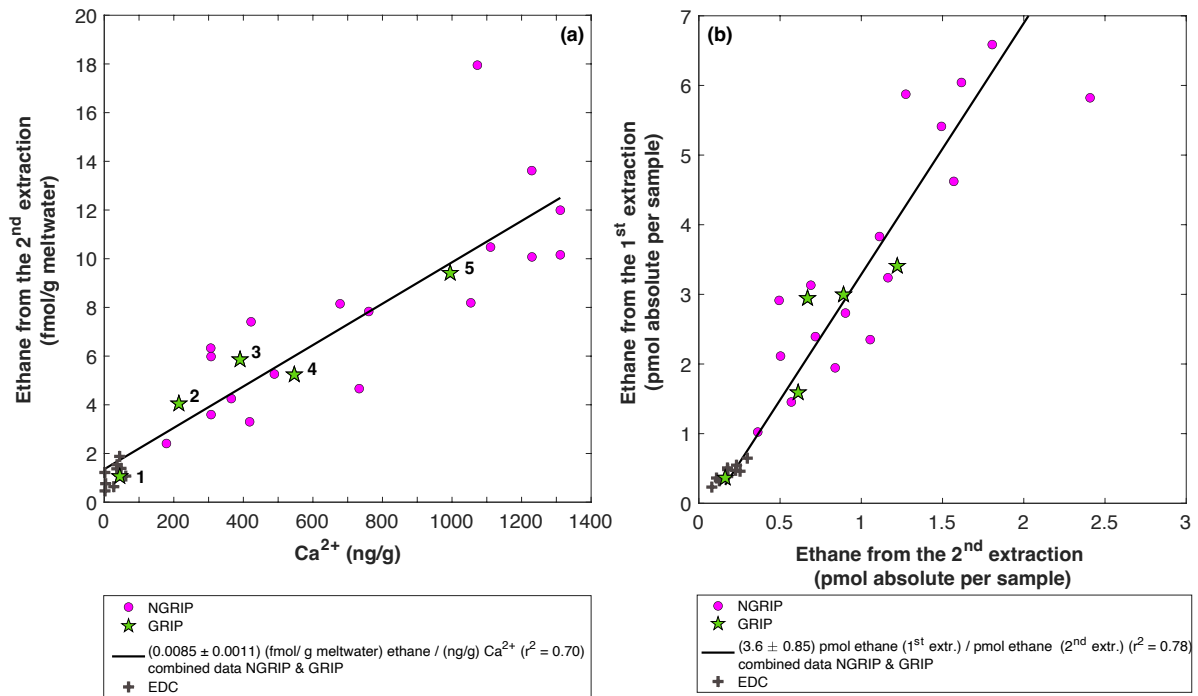
538
539 Overall, excess alkane concentrations increase with increasing Ca²⁺ concentrations, in both the
540 1st and the 2nd extraction. The total alkane production/release, however, decreased in the 2nd
541 extraction, suggesting the progressive exhaustion over time of some reactant necessary for the
542 *in extractu* process. We propose that this reactant co-varies with Ca²⁺ and particulate dust,

543 where Ca^{2+} is of course not a reactant itself and represents only a proxy for higher *in extractu*
 544 production.
 545



546
 547 **Figure 6: NGRIP and GRIP results of excess methane, ethane, and propane from the 2nd extraction. (a)**
 548 Concentrations of methane and ethane and their ratios to each other. **(b)** Concentrations of propane and ethane and
 549 their ratios to each other. Units are given as pmol absolute per sample on the primary axis in black and in ppb
 550 assuming an air volume of 14 mL of the ice core sample on the secondary axis in grey. Crosses indicate the blank
 551 level of the system estimated from 2nd extractions of EDC ice core samples.

552
 553
 554



555
556

557 Figure 7: **GRIP and GRIP results of ethane from the 2nd extraction in relation to the Ca²⁺ concentration**
 558 **and to the 1st extraction.** (a) Produced amount of ethane in the meltwater (fmol/g meltwater) in relation to the
 559 Ca²⁺ concentration in the ice core samples. The numbered GRIP samples are used in Figure C1 to evaluate the
 560 temporal dynamics. Crosses indicate the blank level of the system estimated from 2nd extractions of EDC ice
 561 core samples. (b) Relation of the amount of ethane (pmol) measured in the 1st and 2nd extraction.

562
563
564

3.2 Isotopic composition of excess methane

565 In this section we characterize the isotopic signature of excess methane and explore how we
 566 can use this parameter to better identify its source or production pathway. The evaluation of the
 567 carbon and deuterium isotopic signature of excess methane ($\delta^{13}\text{C-CH}_4(\text{xs})$ and $\delta\text{D-CH}_4(\text{xs})$) is
 568 based on the Keeling-plot approach (Keeling, 1958, 1961; Köhler et al., 2006).

569

3.2.1 $\delta^{13}\text{C-CH}_4$ isotopic signature of excess methane

570
571

572 Figure 8 (left panel) shows the $\delta^{13}\text{C-CH}_4$ results of the 1st extraction. The carbon isotopic
 573 signature of excess CH₄ from the 1st extraction of the ice core sample measurements within one
 574 NGRIP bag are obtained from the y-intercept of the Keeling-plot, representing the excess $\delta^{13}\text{C-CH}_4$
 575 CH₄ value for this bag. Note that the two NGRIP bags 3331 and 3332 are neighbouring bags
 576 and were therefore combined into one Keeling y-intercept. As the individual samples in these
 577 two bags span less than 10 years between each other, they are the same within the age
 578 distribution, and the assumptions for the Keeling-plot approach (see Sec. 2.1) are met. All bags
 579 show agreement in $\delta^{13}\text{C-CH}_4$ signature (y-intercepts) within 2 σ uncertainties. The weighted

580 mean isotopic signature is $(-47.0 \pm 2.9) \text{ ‰}$, with weights assigned by the number of samples
581 that constrained each individual Keeling plot regression line.

582 With the small number of samples that go into the determination of the y-intercept and its error
583 in the Keeling plot for each individual bag, the estimates of the y-intercepts and their error have
584 to be regarded statistically uncertain. However, comparing the results for the individual bags,
585 they all agree within each within the estimated errors. In order to get a more representative
586 value for the isotopic signature of excess CH_4 and its error, we calculate a weighted average
587 for all bags for the y-intercept and its error. Nevertheless, this weighted error may still not be
588 entirely representative because of the small sample number and the true error may likely be
589 somewhat higher.

590

591 Figure 8 (right panel) shows the isotopic results in relation to the amount of CH_4 produced
592 during the 2nd extraction. No atmospheric CH_4 is present during the 2nd extraction and the
593 individual isotopic values in Fig. 8 (right panel) are the directly measured values of excess CH_4
594 without applying the Keeling-plot approach. For a better comparison, the produced CH_4 is
595 shown both in pmol (lower axis in Fig. 8, right panel) and in a mixing ratio CH_4 scale (ppb).
596 The Keeling y-intercept values of the 1st extraction are added in the right panel of Fig. 8.

597

598 The $\delta^{13}\text{C}-\text{CH}_4$ values of the 2nd extraction range between -34 ‰ and -48 ‰ with the mean being
599 $(-41.2 \pm 2.2) \text{ ‰}$. This value appears isotopically somewhat heavier compared to the weighted
600 mean of $(-47.0 \pm 2.9) \text{ ‰}$ inferred from the Keeling analysis, however, is still the same within
601 the 2σ error limits. We note that the measured peak areas for the 2nd extractions are very small
602 and lie outside of the typical range of our gas chromatography mass spectrometry analysis for
603 $\delta^{13}\text{C}-\text{CH}_4$ and we cannot exclude some bias in these results. However, we mimicked these small
604 peak areas with injections of small amounts of standard air and observed no significant bias in
605 the measured $\delta^{13}\text{C}-\text{CH}_4$ values given that the precision of such small peaks is around 2 ‰ .

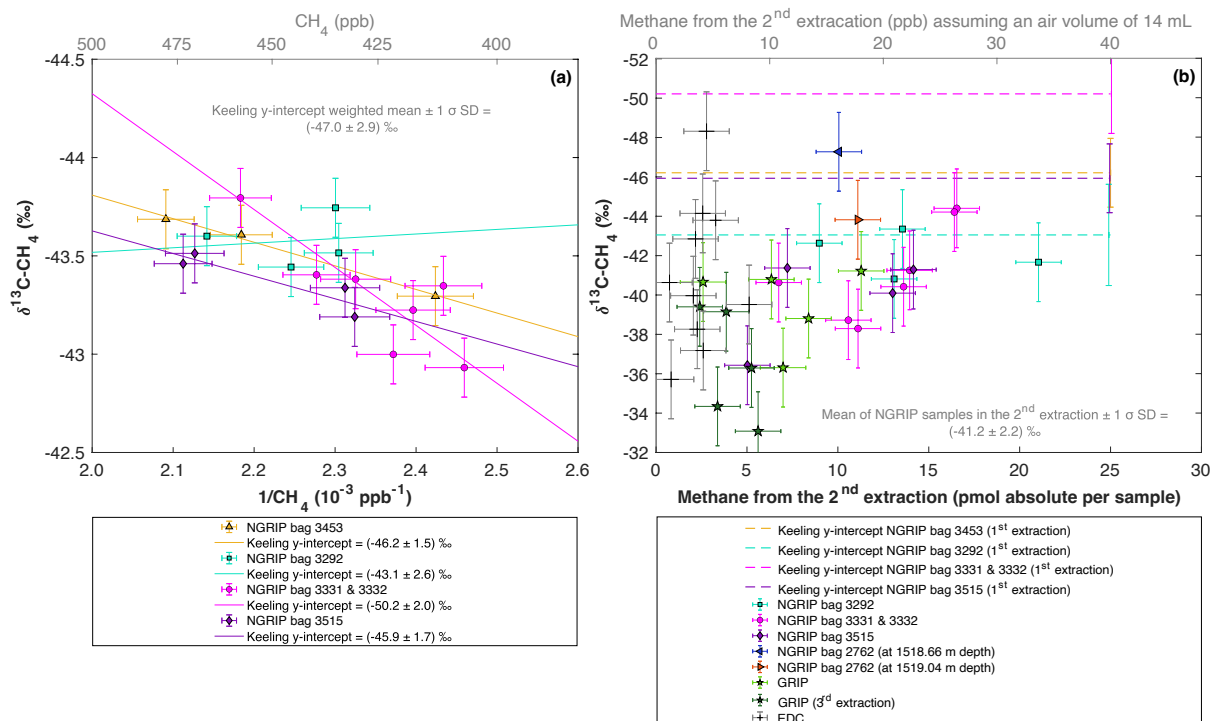
606

607 Another caveat is the considerable blank contribution for CH_4 that we observe for the 2nd
608 extraction. Since Antarctic ice cores do not show a sizable *in extractu* production (Fig. 7,
609 crosses for EDC) we measured EDC samples with the same protocol of a 2nd extraction as for
610 our Greenland samples to provide an upper boundary of this blank. Hence the 2nd extraction of
611 the EDC samples are a conservative blank estimate while the true system blank is lower. As
612 can be seen in Fig. 8 (right panel) the amount of CH_4 measured for these EDC samples (crosses)
613 is on average about 2 pmol (equivalent to about 3 ppb). For comparison, our ice samples from

614 Greenland show a range of about 5 to 20 pmol, indicating a considerable blank contribution in
 615 the 2nd extraction.

616
 617 To estimate the influence of the blank on the isotopic signature that occurs during the 2nd
 618 extraction we used the values from our EDC measurements and applied an isotope mass balance
 619 approach. The $\delta^{13}\text{C-CH}_4$ blank signature obtained from these EDC samples is -39.0 ‰, hence
 620 a few ‰ heavier than the mean $\delta^{13}\text{C-CH}_4$ signature of the excess CH_4 from this 2nd extraction
 621 for the Greenland samples. On average, the correction would shift our NGRIP values towards
 622 lighter (more negative) values by 0.31 ‰. This systematic correction is thus small compared to
 623 the typical measurement precision obtained both from the Keeling-plot approach and the direct
 624 measurement of the $\text{CH}_{4(\text{xs})}$ with the 2nd extraction. As the $\delta^{13}\text{C-CH}_4$ signature of the blank is
 625 close to the NGRIP values, performing a blank correction has only little leverage. Considering
 626 these analytical limitations of our 2nd extraction for $\delta^{13}\text{C-CH}_4$, these findings suggest that
 627 $\text{CH}_{4(\text{xs})}$ produced during the 1st and 2nd extraction has the same $\delta^{13}\text{C-CH}_4$ isotopic signature
 628 within the 2 σ error limits and is likely produced/released by the same process in both
 629 extractions.

630



631
 632 **Figure 8: NGRIP (and GRIP) $\delta^{13}\text{C-CH}_4$ results of the 1st and 2nd extraction measured with the $\delta^{13}\text{C-CH}_4$**
 633 **device. (a) Keeling-plot of $\delta^{13}\text{C-CH}_4$ for NGRIP samples from the five main bags (3292, 3331 & 3332, 3453,**
 634 **3515) measured in the 1st extraction. Colors and symbols indicate individual measurements of the respective bags.**
 635 **Colored lines indicate the corresponding Keeling regression line of each individual bag. (b) $\delta^{13}\text{C-CH}_4$ (‰)**
 636 **values in relation to the amount of methane measured for the 2nd extraction. Units for CH_4 are given as pmol absolute per**
 637 **sample on the primary axis in black, and in ppb assuming an air volume of 14mL of an ice core sample on the**
 638 **secondary axis in grey. Colors and symbols indicate individual measurements of the respective bags. Color-coded**

639 lines indicate the corresponding Keeling y-intercept of each individual bag as measured in the 1st extraction. Grey
640 crosses indicate the blank level of the system estimated from 2nd extractions of EDC ice core samples.

641

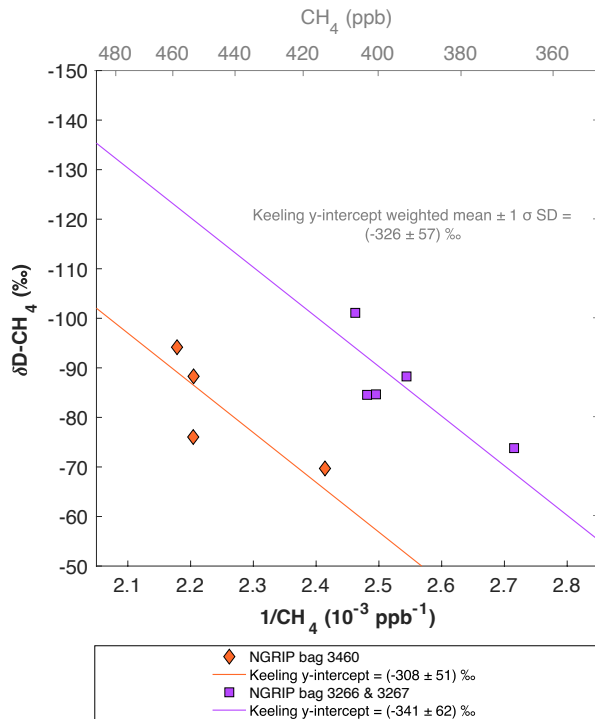
642 **3.2.2 $\delta\text{D-CH}_4$ isotopic signature of excess methane**

643

644 Figure 9 shows the results of the $\delta\text{D-CH}_4$ analyses. Due to the larger sample size required for
645 the $\delta\text{D-CH}_4$ analyses and the sample availability restrictions, only two bags could be measured
646 for $\delta\text{D-CH}_4$. The individual $\delta\text{D-CH}_4$ results obtained from the ice core sample measurements
647 within one NGRIP bag are again combined into one Keeling y-intercept, representing the $\delta\text{D-}$
648 CH_4 value for this bag. NGRIP bag 3460 (orange) reveals a Keeling y-intercept $\delta\text{D-CH}_4$ value
649 of $(-308 \pm 51) \text{‰}$. The two NGRIP bags 3266 and 3267 (purple) are neighbouring bags and
650 were combined into one Keeling y-intercept revealing a $\delta\text{D-CH}_4$ value of $(-341 \pm 62) \text{‰}$. The
651 difference between the two Keeling y-intercepts is within the error limits. Accordingly, we
652 combine the two values to a weighted mean and weighted uncertainty of $(-326 \pm 57) \text{‰}$. As
653 stated above, with the small number of samples that go into the determination of the y-intercept
654 and its error in the Keeling plot for each bag, the estimates of the y-intercepts and their error
655 have to be regarded statistically uncertain.

656 Our results are consistent with the findings of Lee et al. (2020), who used the NGRIP $\delta\text{D-CH}_4$
657 record of Bock et al. (2010b) and the NGRIP $[\text{CH}_4]$ record of Baumgartner et al. (2014) to
658 estimate the $\delta\text{D-CH}_{4(\text{xs})}$ signature in these samples. Assuming a two-component mixture of
659 atmospheric methane and excess methane in their model led to a best estimate of (-293 ± 31)
660 ‰ for $\delta\text{D-CH}_{4(\text{xs})}$ which is within the error limits of our Keeling-plot results.

661



662

663 **Figure 9: NGRIP δD-CH₄ results.** Keeling-plot of δD-CH₄ of NGRIP samples measured with the δD-CH₄ device.
 664 Colors and symbols indicate individual measurements of the respective bags and lines indicate the corresponding
 665 regression of each bag.

666

667 4. Testing the hypotheses explaining excess alkanes

668

669 In Sect. 3 several pieces of evidence for the production/release of excess alkanes in Greenland
 670 ice core samples were collected:

671

672 - We can confirm the observations of Lee et al. (2020) on excess methane in different
 673 Greenland ice cores and its covariance with the amount of mineral dust in the ice.
 674 Despite the different extraction techniques applied (multiple melt-refreeze method in
 675 Lee et al. (2020) versus two subsequent wet extractions in our study), we can further
 676 corroborate that the temporal dynamics of the production/release is on the order of hours
 677 and production/ release occurs when liquid water is present during extraction.

678 - We document for the first time a co-production/release of excess methane, ethane, and
 679 propane, with the observed values for ethane and propane exceeding by far their
 680 estimated past atmospheric background concentrations.

681 - Excess alkanes (methane, ethane, propane) are produced/ released in a fixed molar ratio
 682 of approximately 14:2:1, indicating a common origin.

683 - We further characterize the isotopic composition of excess CH₄ of $\delta^{13}\text{C}-\text{CH}_{4(\text{xs})}$ and $\delta\text{D}-$
684 $\text{CH}_{4(\text{xs})}$ to be $(-47.0 \pm 2.9) \text{‰}$ and $(-326 \pm 57) \text{‰}$ in NGRIP ice core samples,
685 respectively. Within the error limits, our $\delta\text{D}-\text{CH}_{4(\text{xs})}$ results are consistent with the
686 calculated best estimate of $(-293 \pm 31) \text{‰}$ by Lee et al. (2020).
687

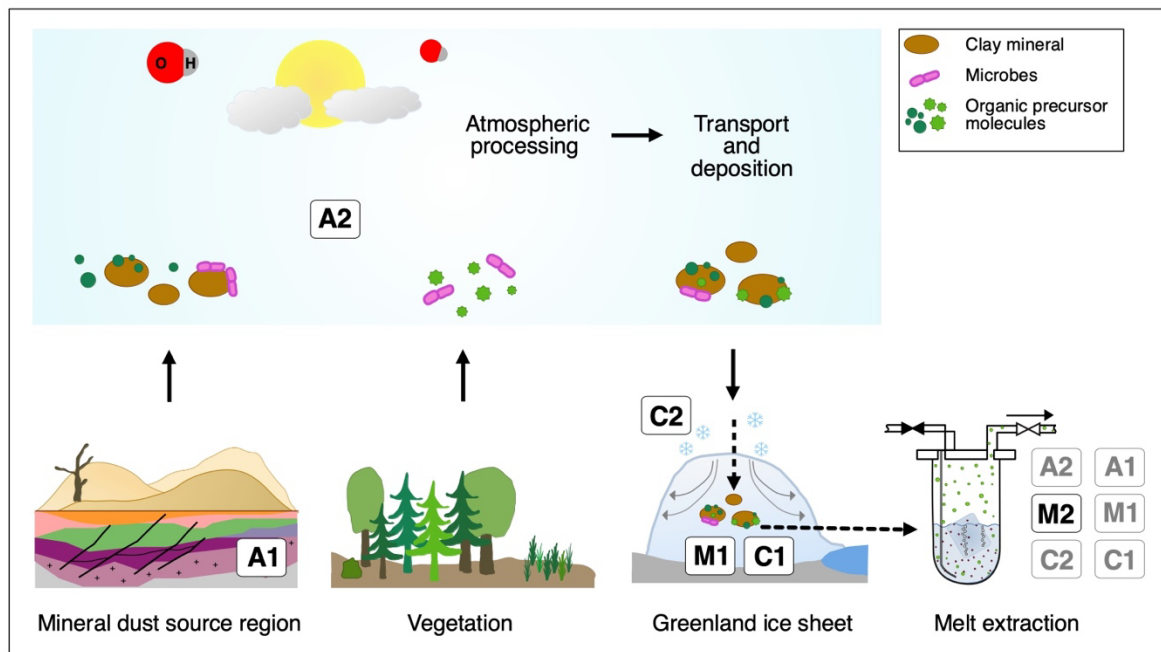
688 In the introduction we presented the hypotheses proposed by Lee et al. (2020) explaining their
689 observations on CH_{4(xs)}. Here we resume the discussion of the original hypotheses and refine
690 them in light of our new data from NGRIP and GRIP measurements. An overview of the
691 possible sources explaining excess alkanes is illustrated in Fig. 10 and Table 1. We discuss in
692 the following three options for the origin of the observed excess alkanes:
693

694 1.) Excess alkanes could be adsorbed on mineral dust particles prior to their deposition on the
695 Greenland ice sheet and released in the laboratory during the prolonged melting process. The
696 adsorption step could happen in the mineral dust source region (East Asian deserts) thereby
697 adsorbing the alkanes from natural gas seeps within the sediment (process marked as A1, see
698 Fig. 10). Alternatively, adsorption of atmospheric alkanes on dust particles can happen anytime
699 starting from the soil surface in the dust source region, during atmospheric transport to the
700 Greenland ice sheet, or within the firn layer before pores are closed-off (A2). The desorption
701 of the adsorbed alkanes happens during the melting process for both cases.
702

703 2.) Excess alkanes could be produced microbially. The production happens either in the ice (in
704 situ), the alkanes are adsorbed on dust particles in the ice and then slowly released during the
705 melting phase in the laboratory (M1). Alternatively, the microbial production happens in the
706 meltwater during the melting process (*in extractu*) (M2). A microbial in situ production in the
707 ice without an adsorption-desorption process was already deemed unlikely by Lee et al. (2020)
708 since it is not compatible with the lack of CH_{4(xs)} in the CFA CH₄ concentration records.

709 3.) Excess alkanes are produced abiotically, e.g. by the decomposition of labile organic
710 compounds. This chemical reaction can happen either in the ice (in situ), where excess alkanes
711 are then adsorbed on dust particles and subsequently released during the melting process (C1),
712 or in the meltwater during extraction (*in extractu*) (C2). An abiotic in situ production in the ice
713 without an adsorption-desorption process can also be ruled out with the CFA evidence.
714

715 We now discuss these mechanisms in detail and evaluate the viability of the different
716 hypotheses in light of our new experimental observations.



718

719 **Figure 10: Overview of the different possibilities explaining excess alkanes in dust-rich Greenland ice.** A
 720 depicts an adsorption process of alkanes on mineral particles, either from natural gas seeps within the sediment
 721 (A1) or from the atmosphere (A2) prior to their deposition on the Greenland ice sheet. This gas is then desorbed
 722 during melting in the laboratory. M depicts a microbial production of excess alkanes, either in the ice (in situ),
 723 followed by adsorption on dust particles in the ice and a subsequent slow desorption process during melting (M1),
 724 or a microbial production in the meltwater (*in extractu*) (M2). C depicts the abiotic/ chemical production of excess
 725 alkanes, either in the ice (in situ) followed by adsorption on dust particles after production in the ice and a
 726 subsequent slow desorption during the melting process (C1), or an abiotic production in the meltwater (*in extractu*)
 727 (C2).

728

729

730 (1) Adsorption/desorption of alkanes on mineral dust particles

731 Depending on where the adsorption occurs, the mineral particles might adsorb alkanes of
 732 different origin and composition. One possibility is that the adsorption already takes place
 733 within the sediment or soil of the dust source region, thus before mineral dust deflation (erosion
 734 of loose material by winds from flat and dry areas; A1). As proposed by Lee et al. (2020), the
 735 major source region of mineral dust arriving in Greenland during the glacial (Taklamakan,
 736 Tarim Basin) are also regions where natural gas seeps reach the surface (Etiopie and Klusman,
 737 2002; Etiopie et al., 2008). In this case, the measured excess alkanes should reflect the seep's
 738 isotopic and alkane composition. Alternatively, adsorption of atmospheric alkanes on the
 739 particles can happen anytime starting from the soil surface, during transport en route to the
 740 Greenland ice sheet after deflation, and within the firn layer before pores are closed-off (A2).
 741 For the scenario A2 the fingerprint (isotopic composition and ratio of alkanes) of the adsorbed
 742 alkanes depends on the past atmospheric composition but could be modulated by selective
 743 fractionation processes during adsorption and desorption.

744

745 To be a viable mechanism for our problem, it requires that the adsorbed alkanes stay strongly
746 bound at the dust particles while desorption is minor both during the atmospheric transport and
747 during the several hundred years the dust particles spend in the porous firn (age of the firn at
748 bubble close-off). During the melting procedure the adsorbed alkanes would then be released
749 from their mineral dust carrier, which in case of Greenland ice from glacial times is
750 predominately consisting of clay minerals from the Taklamakan (and partly also Gobi) desert
751 (Biscaye et al., 1997; Svensson et al., 2000; Ruth et al., 2003). However, additional dust sources
752 exist, with their relative contribution varying with climate conditions (Han et al., 2018; Lupker
753 et al., 2010).

754

755 Several experimental studies showed that clay minerals have a high adsorption capacity and
756 retention potential for alkanes (Sugimoto et al., 2003; Cheng and Huang, 2004; Dan et al., 2004;
757 Pires et al., 2008; Ross and Bustin, 2009; Ji et al., 2012; Liu et al., 2013; Tian et al., 2017).
758 Influencing parameters for an adsorption-desorption process are mainly pressure, temperature,
759 clay mineral type, micropore size, surface area, organic carbon content, and water/ moisture
760 content (Sugimoto et al., 2003; Cheng and Huang, 2004; Dan et al., 2004; Pires et al., 2008;
761 Ross and Bustin, 2009; Ji et al., 2012; Liu et al., 2013; Tian et al., 2017). Most interestingly for
762 us, studies by Sugimoto et al. (2003) and Dan et al. (2004) on the adsorption of CH₄ in
763 micropores on the surface of clay minerals in dried and fresh lake sediment showed that dried
764 sediment still retains CH₄ and that dried and degassed sediment re-adsorbs ambient CH₄ at
765 standard pressure and room temperature. The amount of CH₄ adsorbed in their samples strongly
766 depends on pressure and temperature while increasing temperatures and decreasing pressure
767 lead to stronger desorption. The addition of water/ moisture leads to a rapid desorption of
768 already adsorbed gases (Sugimoto et al., 2003; Dan et al., 2004; Pires et al., 2008; Ji et al.,
769 2012; Liu et al., 2013).

770

771 These observations support the possibility of an adsorption-desorption process for our glacial
772 NGRIP and GRIP ice core samples, where alkanes (from fossil seeps or atmosphere) would be
773 adsorbed on dust particles and desorbed during the extraction when liquid water is present.
774 Independent of the origin of the alkanes (A1 or A2), the amount of alkanes adsorbed on dust
775 deposited onto the Greenland ice sheet by this process would be diminished if the dust particles
776 were already in contact with liquid water during the long-range transport which may lead to a
777 loss of previously adsorbed alkanes. This water contact could occur, for example, already at the

778 dust source, as it is known that the deserts in the Tarim basin receive regular input from water
779 from the surrounding mountain regions that also provide the minerals to the basin that are blown
780 out of the desert afterwards (Ruth et al., 2007).

781

782 To explain the constant ratio of methane, ethane, and propane of 14:2:1 in our samples with an
783 adsorption mechanism, we need to discuss the potential origins of the adsorbed alkanes. First,
784 we find very high relative excess contributions of ethane and propane in our samples, while we
785 see a small excess contribution for methane compared to the atmospheric background. This is
786 not in line with the past atmospheric $\text{CH}_4/(\text{C}_2\text{H}_6+\text{C}_3\text{H}_8)$ ratio where past atmospheric ethane
787 concentrations by Nicewonger et al. (2016) are an order of magnitude smaller (and propane
788 concentrations even less) than the measured concentrations in dust-rich Greenland ice core
789 samples.

790 In contrast, the ratio of methane, ethane, and propane for our samples of approximately 14:2:1,
791 translates into a $\text{CH}_4/(\text{C}_2\text{H}_6+\text{C}_3\text{H}_8)$ ratio of ~ 5 , which is most consistent with a thermogenic
792 origin (see Fig. 11, left panel). However, due to the different adsorption capacity of mineral
793 dust particles, also a fractionation of the three alkanes is to be expected during the adsorption
794 process, which could alter the thermogenic signature.

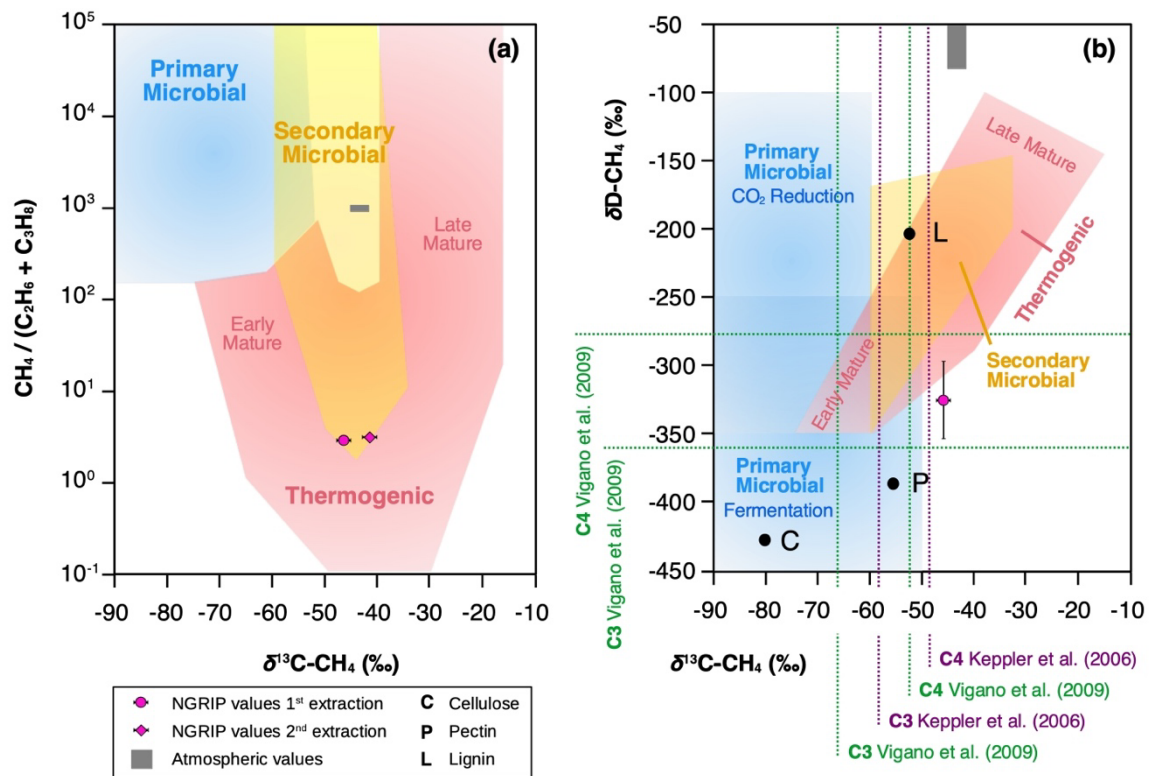
795

796 To further evaluate the adsorption theory in light of our experimental results, we now include
797 the carbon and deuterium isotopic signature of $\text{CH}_{4(\text{xs})}$ in our samples. Our NGRIP samples
798 reveal a $\delta^{13}\text{C}-\text{CH}_{4(\text{xs})}$ value (Keeling y-intercept weighted mean) of $(-47.0 \pm 2.9) \text{‰}$ which is
799 within the error consistent with contemporaneous atmospheric values or with emissions from
800 seeping reservoirs of natural gas. In contrast, our $\delta\text{D}-\text{CH}_{4(\text{xs})}$ measurements on NGRIP samples
801 reveal a very light value (Keeling y-intercept weighted mean) of $(-326 \pm 57) \text{‰}$ and slightly
802 outside of the field of a thermogenic origin (see Fig. 11). The value is similar to the estimate
803 by Lee et al. (2020), which, however, lies inside the field of a thermogenic origin (see Fig. 11).
804 While both the low $\text{CH}_4/(\text{C}_2\text{H}_6+\text{C}_3\text{H}_8)$ ratio and the $\delta^{13}\text{C}-\text{CH}_{4(\text{xs})}$ could be indicative of a
805 thermogenic source (A1), the light $\delta\text{D}-\text{CH}_{4(\text{xs})}$ signature is far away from the atmospheric $\delta\text{D}-$
806 CH_4 value and is borderline in line with typical $\delta\text{D}-\text{CH}_4$ values of a thermogenic origin. Hence,
807 our $\delta\text{D}-\text{CH}_{4(\text{xs})}$ values exclude the atmospheric adsorption scenario A2 and put a question mark
808 after the seep adsorption scenario A1.

809

810 For the seep adsorption scenario A1 to work the dust particles on which the thermogenic gas
811 adsorbed are not allowed to experience any contact with liquid water prior to the analysis in the

812 lab. In other words, if the particles get in contact with liquid water after the adsorption step, the
 813 adsorbed alkanes would desorb from the particles as they do in the laboratory during melting.
 814 Given the occurrence of wet/dry cycles in the source area (Ruth et al., 2007), we question the
 815 plausibility of scenario A1. Moreover, we expect the characteristic desorption time to differ
 816 between the three alkanes, which would be in contradiction to the observation that the alkane
 817 ratios in the 1st and 2nd extraction are the same within the error limits.



818
 819 **Figure 11: Diagrams of genetic fields for natural gas adopted from Milkov and Etiope (2018).** (a) Genetic
 820 diagram of $\delta^{13}\text{C}-\text{CH}_4$ versus $\text{CH}_4/(\text{C}_2\text{H}_6+\text{C}_3\text{H}_8)$. Typical atmospheric values are indicated by a grey-shaded area,
 821 NGRIP values obtained from the 1st and 2nd extraction from this study with a pink dot. (b) Methane genetic diagram
 822 of $\delta^{13}\text{C}-\text{CH}_4$ versus $\delta\text{D}-\text{CH}_4$. Values for cellulose (C), lignin (L) and pectin (P) from Vigano et al. (2009) and mean
 823 values for C3 and C4 plants, respectively, from studies by Keppler et al. (2006) and Vigano et al. (2009) are added.

824
 825
 826
 827

828 (2) Microbial production

829 The second process that we take into consideration is the microbial production of excess alkanes
 830 through methanogenic microbes. Here we must again differentiate between two scenarios:
 831 microbial production can either take place in the ice sheet (in situ) by extremophile microbes.
 832 This process requires that in situ produced excess alkanes are then adsorbed onto dust particles

833 in the ice and subsequently slowly desorbed during melting when in contact with liquid water
834 (M1). Or the production takes place during the melt extraction when methanogens can
835 metabolize in liquid water (*in extractu*; M2). Lee et al. (2020) already excluded a “simple” in
836 situ production of excess CH₄ (microbial in situ production in the ice without an adsorption-
837 desorption process; M0) and this option will therefore not be further discussed here.

838 Our ratios of excess methane/ethane/propane in NGRIP and GRIP samples add another piece
839 of corroborating evidence that excess alkanes are not produced microbially. The main microbial
840 production process of methane, the decomposition of organic precursors in an anaerobic
841 environment by archaea, also co-produces ethane and propane, however only in marginal
842 amounts. The typical methanogenesis yields >200 times more methane than ethane and propane
843 (Bernard et al., 1977; Milkov and Etiope, 2018) while we find a molar ratio of methane to
844 ethane to propane of 14:2:1 in our samples. This renders a microbial production pathway (in
845 situ and *in extractu*, i.e. M1 and M2) unlikely. Moreover, a microbial production of CH₄ is
846 unlikely in view of the $\delta^{13}\text{C-CH}_{4(\text{xs})}$ signature which is too heavy for microbial CH₄.

847
848 Apart from these quantitative limitations of microbial CH₄ in situ production in ice, there is
849 evidence from the “microbial inhibition experiment“ by Lee et al. (2020) against microbial
850 production of alkanes during the melt extraction. Lee et al. (2020) tested whether biological
851 CH_{4(xs)} production in the meltwater was inhibited when the ice core samples were treated with
852 HgCl₂. As CH_{4(xs)} was still observed in the poisoned samples and as it seems unlikely that
853 microbes are resistant to HgCl₂, this experiment questions the hypothesis of microbially
854 produced CH_{4(xs)} also during extraction (*in extractu*).

855
856 We conclude that regardless of the location of the production, in situ or *in extractu*, the
857 fingerprint of the excess alkanes in our samples (heavy $\delta^{13}\text{C-CH}_{4(\text{xs})}$ signature and low
858 CH₄/(C₂H₆+C₃H₈) ratio) essentially rules out a microbial source and another (abiotic?) process
859 for excess alkane production is likely to exist.

860

861 **(3) Abiotic/ chemical production**

862 In this last section we consider an abiotic or chemical process to be responsible for the observed
863 excess alkanes, where excess alkanes would be produced through the abiotic decomposition of
864 labile organic compounds in the meltwater (C2). We question an abiotic in situ production in
865 the ice (C1) as it would require the quantitative adsorption of the in situ produced alkanes onto
866 mineral dust particles but not the atmospheric CH₄ that is available in the ice otherwise.

867 However, as the location of an in situ excess CH₄ production in the ice is not the same as the
868 location of the bubble or clathrates in the ice, this argument is not able to exclude this
869 hypothesis. However, given the age of the ice that allows for permeation of gases on the grain
870 scale and the recrystallization of the ice during that time, which both could bring the
871 atmospheric CH₄ in contact with the dust particles, we feel this process is less plausible than a
872 potential C2 mechanism. Moreover (as mentioned before), in view of the expected different
873 desorption characteristics of the three alkanes, we would expect different alkane ratios in the
874 1st and 2nd extraction, which is not the case. Accordingly, a direct abiotic production during
875 melting appears to be more likely than a desorption process.

876
877 Organic precursors for this abiotic production during extraction could be any organic matter
878 (either microbial or plant-derived). As the amount of excess alkanes is tightly coupled to the
879 amount of dust, we assume that these organic compounds are attached to dust particles. This
880 “docking” of the organic precursor onto the mineral dust could happen already in the dust
881 source region involving organic material available at the surface. Or it could happen by
882 adhering of volatile organic molecules or secondary organic aerosols from the atmosphere to
883 the mineral dust aerosol either before deflation at the source region or during transport to
884 Greenland.

885
886 We consider this pathway plausible, as in recent years the prevailing paradigm that methane is
887 only produced by methanogenic archaea under strictly anaerobic conditions has been
888 challenged. Several experimental studies demonstrated that methane can also be released from
889 dried soils (Hurkuck et al., 2012; Jugold et al., 2012; Wang et al., 2013; Gu et al., 2016), fresh
890 plant matter and dry leaf litter (Keppler et al., 2006; Vigano et al., 2008, 2009, 2010; Bruhn et
891 al., 2009; Derendorp et al., 2010, 2011), different kinds of living eukaryotes (plants, animals
892 and fungi) (Liu et al., 2015), single organic structural components (McLeod et al., 2008;
893 Messenger et al., 2009; Althoff et al., 2014) and in fact under aerobic conditions. Most of these
894 studies focused on methane, however, there is also evidence for simultaneous formation of other
895 short-chain hydrocarbons like ethane and propane (McLeod et al., 2008; Derendorp et al., 2010,
896 2011). At least three mechanisms have been identified to be relevant: i) photo-degradation, ii)
897 thermal degradation, or iii) degradation by the reaction with a reactive oxygen species (ROS)
898 (Schade et al., 1999; Wang et al., 2017). Common to all three pathways is a functional group
899 (for example a methyl or ethyl group) that is cleaved from the organic precursor molecule. Key
900 parameters that control the production of abiotic methane are mainly temperature, UV radiation,

901 water/ moisture, and the type of organic precursor material (Vigano et al., 2008; Derendorp et
902 al., 2010, 2011; Hurkuck et al., 2012; Jugold et al., 2012; Wang et al., 2013, 2017).

903

904 Recent findings demonstrated the large variety of potential organic precursors for abiotic trace
905 gas formation. For methane formation, the plant structural components pectin and lignin have
906 been identified in many studies as a precursor in different plant materials. Pectin and lignin
907 contain methoxyl-groups in two different chemical types, ester methoxyl (present in pectin) and
908 ether methoxyl (present in lignin) (Keppler et al., 2006, 2008; McLeod et al., 2008; Messenger
909 et al., 2009; Bruhn et al., 2009; Vigano et al., 2008; Hurkuck et al., 2012; Liu et al., 2015; Wang
910 et al., 2017). Ester methyl groups of pectin were also discovered as precursor for ethane
911 formation (McLeod et al., 2008). Overall, pectin makes up a large fraction of the primary cell
912 wall mass of many plants, thus, representing a large reservoir available as precursor for abiotic
913 alkane formation (Keppler et al., 2006; Mohnen et al., 2008; Vigano et al., 2008, 2010; McLeod
914 et al., 2008), and may be present in sufficient quantities in our ice core samples attached to
915 mineral dust particles. CH₄ production was also detected from cellulose even though it does not
916 contain methoxyl groups suggesting that other carbon moieties of polysaccharides might allow
917 abiotic CH₄ formation (Keppler et al., 2006; Vigano et al., 2008). In addition, poly-unsaturated
918 fatty acids in plant membranes are suggested to play a key role not only in the formation of
919 methane but also for ethane and propane (John and Curtis, 1977; Dumelin and Tappel, 1977;
920 Derendorp et al., 2010, 2011). Further, sulfur-bound methyl groups of methionine are an
921 important precursor for abiotic CH₄ formation in fungi (Althoff et al., 2014).

922

923 Considerably different emission rates were found for the same amount but different type of
924 organic substances leading to the conclusion that abiotic emissions are strongly dependent on
925 the type of organic precursor material or single structural components (Keppler et al., 2006;
926 McLeod et al., 2008; Vigano et al., 2008; Messenger et al., 2009; Hurkuck et al., 2012). Other
927 factors such as leaf and cell wall structure (McLeod and Newsham, 2007; Watanabe et al.,
928 2012; Liu et al., 2015) and the organic carbon content (Hurkuck et al., 2012) are suggested to
929 influence this process, too.

930

931 To explain the observed excess alkanes in dust-rich Greenland ice core samples by an abiotic
932 production through the decomposition of labile organic compounds requires adequate quantities
933 of organic precursors within the ice core samples. Certainly, such material is present in
934 Greenland ice, but currently, there is no record on the amount and type of organic substances

935 available. We have some limited information from occasional Greenland ice core samples in
936 which different types of organic substances were detected (Giorio et al., 2018, and references
937 therein), but it does not allow for an overarching interpretation for our ice samples. A NGRIP
938 record on formaldehyde and a GRIP record on acetate and formate exists (Fuhrer et al., 1997),
939 which suggest lower levels during the glacial, but as we do not know which organic precursors
940 lead to the excess CH₄ productions this observation is only of limited value.

941

942 We may also question whether a perfect record of eligible precursor molecules could exist at
943 all. As we observe that precursor substances are labile and quickly decompose when in contact
944 with liquid water, a direct measurement of these substances might not be possible but only for
945 similar, non-reactive substances, which are then not qualified as precursors for the reaction
946 observed. The problems of sampling, analysis and interpretation of organic material in polar
947 ice are well summarized and expounded in Giorio et al. (2018).

948

949 In any case, it appears likely that the mineral dust carries along soil organic matter or plant
950 residues or accumulates organic aerosols as a result of organic aerosol aging during transport.
951 In our data we see a relationship between the amount of mineral dust within the ice core samples
952 and the amount of excess alkanes. As the amount of excess alkanes per Ca²⁺ (or mass of dust)
953 is variable, this suggests that mineral dust is just a carrier for (a variable amount of) organic
954 substances but does not account for the production of excess alkanes itself. The dust content
955 within the ice core sample can only serve as a rough estimate of organic precursor availability
956 and whether an abiotic production from organic precursor substances is likely to occur during
957 extraction.

958

959 Again, our experiments can shed some light on the viability of this pathway for excess alkane
960 production. If we assume that the dust-related organic matter in the ice represents a reservoir
961 available for abiotic production, then the decomposition continues until all functional groups
962 are cleaved from their organic precursor molecules and released as excess alkanes. Once the
963 reservoir is emptied, excess alkane production ceases (Derendorp et al., 2010, 2011). In line,
964 we interpret that the decrease in the amount of measured excess alkanes from the 1st to the 2nd
965 extraction may result from an exhaustion of the precursor reservoir. The reaction time is slow
966 enough to allow for the continuing production during the second extraction but too slow for a
967 detectable production during continuous flow analysis of CH₄, where the water phase is present
968 only for less than two minutes before gas extraction. The significantly reduced production

969 during the 2nd extraction in our samples shows that the time scale for this process is hours (see
970 Fig. C1) until the reservoir of functional groups is depleted. We note that this implies that the
971 amount of excess alkanes is strongly dependent on the time span when liquid water is in contact
972 with the dust, which varies among the methods used for CH₄ analyses. Thus, any excess CH₄
973 in measurements from different labs performed under different conditions may differ.

974

975 To explain an abiotic alkane production, certain conducive boundary conditions must be met.
976 The most important parameters that control non-microbial trace gas formation are temperature
977 and UV radiation. This was demonstrated in many field and laboratory experiments (Keppler
978 et al., 2006; McLeod et al., 2008; Vigano et al., 2008, 2009; Messenger et al., 2009; Bruhn et
979 al., 2009; Derendorp et al., 2010, 2011; Hurkuck et al., 2012; Jugold et al., 2012; Wang et al.,
980 2017). Generally, increasing temperatures lead to exponentially increasing CH₄ emissions
981 (Vigano et al., 2008; Bruhn et al., 2009; Wang et al., 2013; Liu et al., 2015). The same behaviour
982 was observed for ethane and propane with very low emissions at ambient temperatures (20-
983 30°C) and a maximum at 70°C (McLeod et al., 2008; Derendorp et al., 2010, 2011). At constant
984 temperatures emission rates decreased over time, which is at high temperatures on the timescale
985 of hours and at ambient temperatures of months. Even after months, some production was
986 observed, pointing to a slowly depleting reservoir of organic precursors (Derendorp et al., 2010,
987 2011). Increasing emissions observed at temperatures >40°C were also used as indicator to
988 exclude the possibility of enzymatic activity, as the denaturation of enzymes would lead to
989 rapidly declining emissions at higher temperatures (Keppler et al., 2006; Derendorp et al., 2011;
990 Liu et al., 2015). We note that our sample extraction takes place at 0°C or a few °C above,
991 hence, temperature conditions during the extraction are not conducive of the type of abiotic
992 alkane production as observed in the studies listed above. Whether the cool temperature of the
993 meltwater during extraction inhibits abiotic reaction is difficult to say. Derendorp et al. (2010,
994 2011) observed a much lower temperature dependency of C₂-C₅ hydrocarbon emissions from
995 ground leaves than whole leaves, which might also apply to our samples with very fine
996 fragments of organic substances attached to dust particles.

997

998 Besides the strong relationship to temperature also UV irradiation seems to have a substantial
999 effect on abiotic production. Studies on irradiated samples (dry and fresh plant matter, plant
1000 structural components) showed a linear increase in methane emissions, while UV-B irradiation
1001 seems to have a much stronger effect on the release compared to UV-A (Vigano et al., 2008;
1002 McLeod et al., 2008; Bruhn et al., 2009; Jugold et al., 2012). The influence of visible light (400-

1003 700 nm), however, seems controversial (Keppler et al., 2006; Bruhn et al., 2009; Austin et al.,
1004 2016). Further, samples that were heated and irradiated show a different emission curve than
1005 just heated samples, indicating that irradiation changes the temperature dependency, in turn
1006 pointing to the fact that different chemical pathways exist (Vigano et al., 2008).

1007 In dark experiments on plant material at different temperatures CH₄ emissions were still
1008 observed, while again higher temperatures revealed much higher emissions, emphasizing the
1009 strong temperature dependency also without UV irradiation (Vigano et al., 2008; Wang et al.,
1010 2008; Bruhn et al., 2009). The release of ethane along with methane from pectin was also
1011 stimulated under UV radiation (McLeod et al., 2008).

1012
1013 Regarding our measurements, the sample vessel in the $\delta^{13}\text{C}$ -CH₄ device is encased by a UV
1014 blocker foil absorbing the shortwave (<600 nm) emissions from the heating bulbs when melting
1015 the ice sample, while in the δD -CH₄ device, the sample vessel is completely shielded from light
1016 (Sect. 2.2 and 2.3). Two NGRIP ice core samples were measured with the $\delta^{13}\text{C}$ -CH₄ device in
1017 the dark (“dark extraction”) showing the same amount of excess alkanes as the regular
1018 measurements at day light. This indicates that light >600 nm has no influence on an *in extractu*
1019 reaction during our measurements.

1020
1021 We stress that although we can exclude a direct UV effect during melting, it is possible that UV
1022 irradiation during dust aerosol transport to Greenland and within the upper snow layer after
1023 deposition until the snow gets buried into deeper layers may precondition organic precursors
1024 attached to dust to allow for alkane production to occur during the melt extraction. In particular,
1025 the first step of the reaction (excitation of the homolytic bond of a precursor compound) may
1026 start already in the atmosphere or in the snow where UV radiation is available. Within the ice
1027 sheet the reaction may be paused (“frozen reaction”) and the total reaction pathway is only
1028 completed during the melting process when liquid water is present.

1029
1030 Finally, we consider the role of reactive oxygen species in an abiotic production pathway. ROS
1031 are widely produced in metabolic pathways during biological activity but also during
1032 photochemical reactions with mineral oxides (Apel and Hirt, 2004; Messenger et al., 2009;
1033 Georgiou et al., 2015). Through their high oxidative potential, ROS can cleave functional
1034 groups from precursor compounds. Several studies have demonstrated this mechanism for the
1035 production of abiotic CH₄ in soils and plant matter (McLeod et al., 2008; Messenger et al.,
1036 2009; Althoff et al., 2010, 2014; Jugold et al., 2012; Wang et al., 2011, 2013) and for other
1037 trace gases such as CO₂, ethane, and ethylene from plant pectins (McLeod et al., 2008). UV

1038 radiation or thermal energy has no direct influence on the degradation process by the reaction
1039 with ROS, however, it might also be a stimulating factor and evoke further indirect reactions.
1040 For instance, UV radiation can lead to changes in plants which in turn lead to ROS generation
1041 (Liu et al., 2015). It was demonstrated that UV radiation induces the formation of organic
1042 photosensitizers or photo-catalysts which increase CH₄ emissions from pectin (Messenger et
1043 al., 2009) and clay minerals. For example, the formation of hydroxyl radicals from
1044 montmorillonite and other clay minerals upon UV (and visible light) irradiation shows that
1045 clays might play a significant role in the oxidation of organic compounds on their surface
1046 (Katagi, 1990; Wu et al., 2008; Kibanova et al., 2011).

1047
1048 It has been proven that the species type and the overall amount of ROS available for, or involved
1049 in a reaction, has a significant effect on the amount of emissions through such a process (Jugold
1050 et al., 2012; Wang et al., 2013, 2017). For the production of methane (and ethane), hydrogen
1051 peroxide (H₂O₂) and hydroxyl radicals have been proven to be the prominent species
1052 (Messenger et al., 2009; Althoff et al., 2010; Wang et al., 2011, 2013; Jugold et al., 2012;
1053 McLeod et al., 2008). Such ROS could be already present in the snow and ice or being produced
1054 in the meltwater. For example, H₂O₂ can be unambiguously detected in Greenland Holocene
1055 ice using CFA, however, H₂O₂ in dusty glacial ice is mostly below the detection limit, likely
1056 due to oxidation reactions in the ice sheet or during melt extraction.

1057
1058 In summary, we believe that in our case of excess alkane production/ release in the meltwater
1059 at low temperatures and without any UV irradiation, the ROS-induced mechanism appears
1060 possible. In experiments with plant pectin McLeod et al. (2008) observed not only CH₄ but also
1061 ethane and found a methane to ethane production ratio of around 5 which is similar to our value
1062 of around 7. Accordingly, we see that a ROS-induced production pathway has the potential to
1063 explain excess alkanes in our samples, however, little is known about ROS chemistry in ice in
1064 particular for reactions with organic precursors and more research is needed to understand the
1065 role of ROS in organic decomposition in ice. Another alternative to the two-stage reaction
1066 pathway with ROS would be a reaction catalyzed in the meltwater by dust-derived transition
1067 metals. This has been observed for example for the oxidation of SO₂ in water-activated aerosol
1068 particles (Harris et al., 2013), but to our knowledge it has not been described in the literature
1069 for alkane production via organic precursors so far. Accordingly, we can only speculate on this
1070 pathway at the moment.

1071

1072

1073 Another key parameter influencing all abiotic pathways might be the presence of liquid water
1074 or moisture. In experiments testing the hypothesis of non-microbial CH₄ formation in different
1075 soil samples, it was demonstrated that adding water/moisture led to an up to eight-fold increase
1076 in CH₄ emissions (Hurkuck et al., 2012; Jugold et al., 2012; Wang et al., 2013). It is
1077 hypothesized that the presence of liquid water or moisture stimulates (in addition to heating or
1078 UV radiation) the cleaving process of a functional group from the primary precursor and
1079 therefore increases the production of CH₄. With respect to our observations on NGRIP and
1080 GRIP samples the presence of water seems to be a fundamental parameter influencing the
1081 second step of a “frozen reaction” *in extractu* process, where the duration of water presence
1082 plays an important role.

1083

1084 A final puzzle piece for a possible abiotic methane production comes from our dual isotopic
1085 fingerprints of the excess CH₄. As illustrated in Fig. 11 (right panel) our $\delta\text{D-CH}_4(\text{xs})$ signature
1086 lies well within the distribution of the hydrogen isotopic composition of CH₄ produced from
1087 potential organic precursors. For $\delta^{13}\text{C}$ our values lie outside and on the heavier side of the
1088 carbon isotope signature spectrum.

1089

1090 We conclude that despite our inability to pinpoint the exact organic precursors that lead to
1091 abiotic excess alkane production during the melt extraction of our ice samples, both the ratio of
1092 the excess alkanes as well as the isotopic signature of excess CH₄ is generally in line with this
1093 pathway. Thus, without further contradicting evidence from targeted studies on organic
1094 precursors in ice core samples and their chemical degradation, we believe that the ROS-induced
1095 production pathway is to date the most likely explanation for the observed excess alkanes
1096 during extraction. However, we cannot completely rule out an adsorption-desorption process
1097 of thermogenic gas on dust particles.

1098

1099

1100

1101

1102

1103

1104

1105

1106

1107

1108

1109

1110

1111

1112

1113 Table 1: **Overview of the different hypotheses explaining the possible sources for excess alkanes (as**
 1114 **illustrated in Figure 10) in relation to our experimental observations.** A green checkmark indicates that the
 1115 observation is in line with the respective mechanism, a black cross indicates that the observation is in not line with
 1116 the respective mechanism. A grey shaded area means that this observation does not apply or does not affect the
 1117 respective mechanism.

1118

	(1) ADSORPTION- DESORPTION OF THERMOGENIC/ ATMOSPHERIC GAS		(2) MICROBIAL PRODUCTION			(3) ABIOTIC/ CHEMICAL PRODUCTION	
	A1	A2	M0	M1	M2	C1	C2
Correlation to Ca ²⁺ / mineral dust	✓	✓	✓	✓	✓	✓	✓
Alkane pattern	✓	✗	✗	✗	✗	(✓)	(✓)
CFA evidence			✗				
$\delta^{13}\text{C}-\text{CH}_{4(x\text{s})}$	✗	✓	✗	✗	✗	(✓)	(✓)
$\delta\text{D}-\text{CH}_{4(x\text{s})}$	✓	✗	✓	✓	✓	(✓)	(✓)
$\delta\text{D}-\text{CH}_{4(x\text{s})}$ estimated by Lee et al. (2020)	✓	✗	✓	✓	✓	(✓)	(✓)
Poisoning experiment by Lee et al. (2020)					✗		

1119

1120

1121 5. Conclusions and Outlook

1122

1123 The comparison of methane records from ice cores samples measured with different melt
 1124 extraction techniques requires careful consideration and interpretation. Non-atmospheric
 1125 methane contributions to the total methane concentration were discovered in specific Greenland
 1126 ice core sections pointing to a process occurring during the wet extraction. To better assess this
 1127 finding, we measured new records of [methane], [ethane], [propane], $\delta\text{D}-\text{CH}_4$, and $\delta^{13}\text{C}-\text{CH}_4$
 1128 on discrete NGRIP and GRIP ice core samples using two different wet extraction systems. With
 1129 our new data we confirm the production of $\text{CH}_{4(x\text{s})}$ in the meltwater and quantify its dual isotopic
 1130 signature. With the simultaneous detection of ethane and propane we discovered that these
 1131 short-chain alkanes are co-produced in a fixed molar ratio pointing to a common production
 1132 pathway. With our 2nd extraction we constrained the temporal dynamics of this process, which
 1133 occurs on the timescale of hours.

1134

1135 Based on our new experimental data we provide an improved assessment of potential
1136 mechanisms that could explain the observed variations in NGRIP and GRIP ice samples. A
1137 microbial CH₄ production represents an obvious candidate, but regardless of whether this CH₄
1138 is produced in situ or *in extractu*, several lines of evidence gained from our measurements (low
1139 CH₄/(C₂H₆+C₃H₈) ratio, heavy $\delta^{13}\text{C-CH}_{4(\text{xs})}$ signature) demonstrate that the fingerprint of the
1140 produced excess alkanes is unlikely of microbial origin. Also an adsorption-desorption process
1141 of atmospheric or thermogenic CH₄ on dust particles does not match many of our observations
1142 and is therefore unlikely. However, with the current knowledge we cannot definitely exclude
1143 such an adsorption of thermogenic gas to be responsible for the observed excess alkane levels
1144 in our samples.

1145

1146 At present we favor to explain the formation of excess alkanes by abiotic decomposition of
1147 organic precursors during prolonged wet extraction. Such an abiotic source for methane and
1148 other short-chain alkanes was discovered previously in other studies (Keppler et al., 2006;
1149 Vigano et al., 2008, 2009, 2010; Messenger et al., 2009; Hurkuck et al., 2012; Wang et al.,
1150 2013, and others listed above) using different organic samples, e.g. from plant or soil material,
1151 however, this process has not been connected to excess CH₄ production during ice core
1152 analyses. This process matches many of our observations, and such a mechanism can be
1153 responsible for excess alkanes in Greenland ice core samples. To better assess a potential abiotic
1154 production process in ice analyses the most important questions to solve in the future are: What
1155 are the specific precursor substances? Which parameters control an abiotic production during
1156 wet extractions? How does the fixed molar ratio between methane, ethane, and propane come
1157 about in this process? And finally, in which way is this excess alkane production causally
1158 related to the amount of mineral dust within the ice sample?

1159

1160 Identifying a specific reaction pathway that leads to the short-chain alkanes with their observed
1161 ratios would certainly benefit from identifying targeted organic precursor substances in the ice.
1162 However, detecting these postulated organic precursors in the ice core is inherently difficult as
1163 these compounds are very labile in water as our experiments demonstrated that after about 30
1164 min only a fraction of these compounds remains in the meltwater while the majority already
1165 reacted to excess alkanes. Future studies may also focus on further isotope measurements ($\delta^{13}\text{C-}$
1166 CH₄ and $\delta\text{D-CH}_4$) including isotope labeling experiments providing an option to
1167 unambiguously detect methane produced during the measurement procedure in a commonly

1168 used wet extraction technique, and again, to uncover potential reaction mechanisms for CH_{4(xS)}
1169 production.

1170

1171 To better assess the viability of the alternative hypothesis of a release of previously adsorbed
1172 alkanes from dust particles (scenario A1 and A2) during the extraction, dust particles from the
1173 Taklamakan or Gobi desert need to be tested whether they contain relevant amounts of adsorbed
1174 alkanes that are released when in contact with liquid water. A second step could be to expose
1175 such dust samples to high levels of alkanes to mimic the adsorption process of natural gas seeps.
1176 It also needs to be shown that the adsorbed alkanes stay adsorbed on the dust particles for a
1177 prolonged time (months, ideally years) after exposing the particles to ambient air and that
1178 droplet and ice nucleation during aerosol transport does not lead to a loss of the previously
1179 adsorbed CH₄. To quantify any isotopic fractionation involved with the ad- and desorption step,
1180 $\delta^{13}\text{C-CH}_4$ and $\delta\text{D-CH}_4$ analyses will be most valuable.

1181

1182 Finally, our studies clearly show that the published Greenland ice core CH₄ record is biased
1183 high for selected (glacial, dust-rich) time intervals and needs to be corrected for the excess CH₄
1184 contribution. This is particularly important for studies of the IPD in CH₄ and stable isotope
1185 ratios of methane. Methodological ways to remedy excess methane (and ethane and propane)
1186 in future measurements of atmospheric [CH₄] from air trapped in ice cores could be to use
1187 continuous online CH₄ measurements, which apparently avoid sizeable CH_{4(xS)} production. But
1188 also dry extraction methods and sublimation techniques for discrete samples, which are
1189 expected to avoid *in extractu* production by evading the melting phase, could be used. Finally,
1190 our own $\delta^{13}\text{C-CH}_4$ device, which allows to measure $\delta^{13}\text{C-CH}_4$ as well as methane, ethane, and
1191 propane concentrations from the same sample, can be used to correct the measured CH₄ values
1192 making use of the co-production of the other two alkanes.

1193

1194 CH_{4(xS)} needs to be corrected for when interpreting the already existing discrete CH₄ records
1195 and its stable isotopes in dust-rich intervals in Greenland ice core samples. Impact of CH_{4(xS)} on
1196 interpreting past atmospheric [CH₄] will only slightly affect radiative forcing reconstructions,
1197 however, it will have a significant effect on the assessment of the global CH₄ cycle and in
1198 particular on the hemispheric CH₄ source distribution which is based on the IPD. We observe
1199 that in some intervals, CH_{4(xS)} is in the same range as the previously reconstructed IPD implying
1200 that correcting for CH_{4(xS)} will lower the IPD considerably and hence lower also the relative
1201 contribution of northern hemispheric sources at those times. We see that there is an urgent need

1202 to reliably revisit Greenland ice core CH₄ records for the excess CH₄ contribution. In future
1203 work we aim to establish an applicable correction for excess methane (CH_{4(xs)}, $\delta^{13}\text{C-CH}_{4(xs)}$,
1204 $\delta\text{D-CH}_{4(xs)}$) in existing records using the co-production ratios of methane, ethane, and propane,
1205 the isotope mass balance of excess and atmospheric CH₄ in ice core samples as well as the
1206 overall correlation of excess CH₄ with the mineral dust content in the ice.

1207

1208

1209

1210

1211

1212

1213

1214

1215

1216

1217

1218

1219

1220

1221

1222

1223

1224

1225

1226

1227

1228

1229

1230

1231

1232

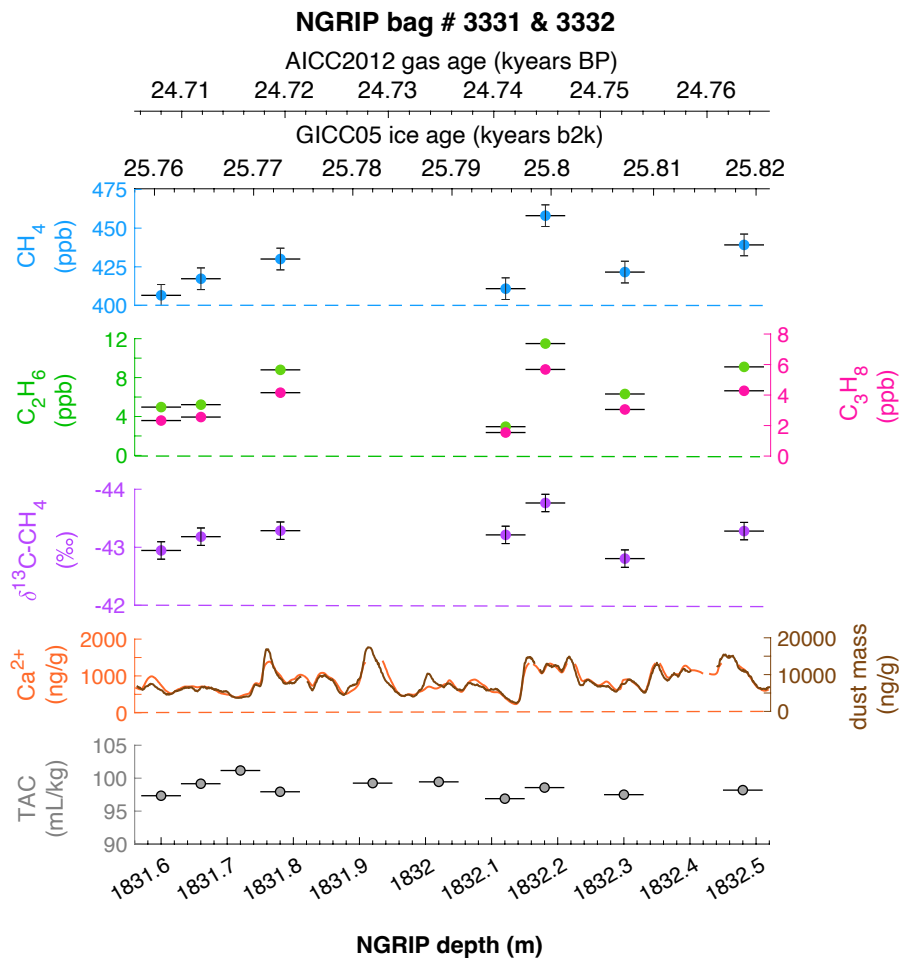
1233

1234

1235

1236 **Appendix A**

1237

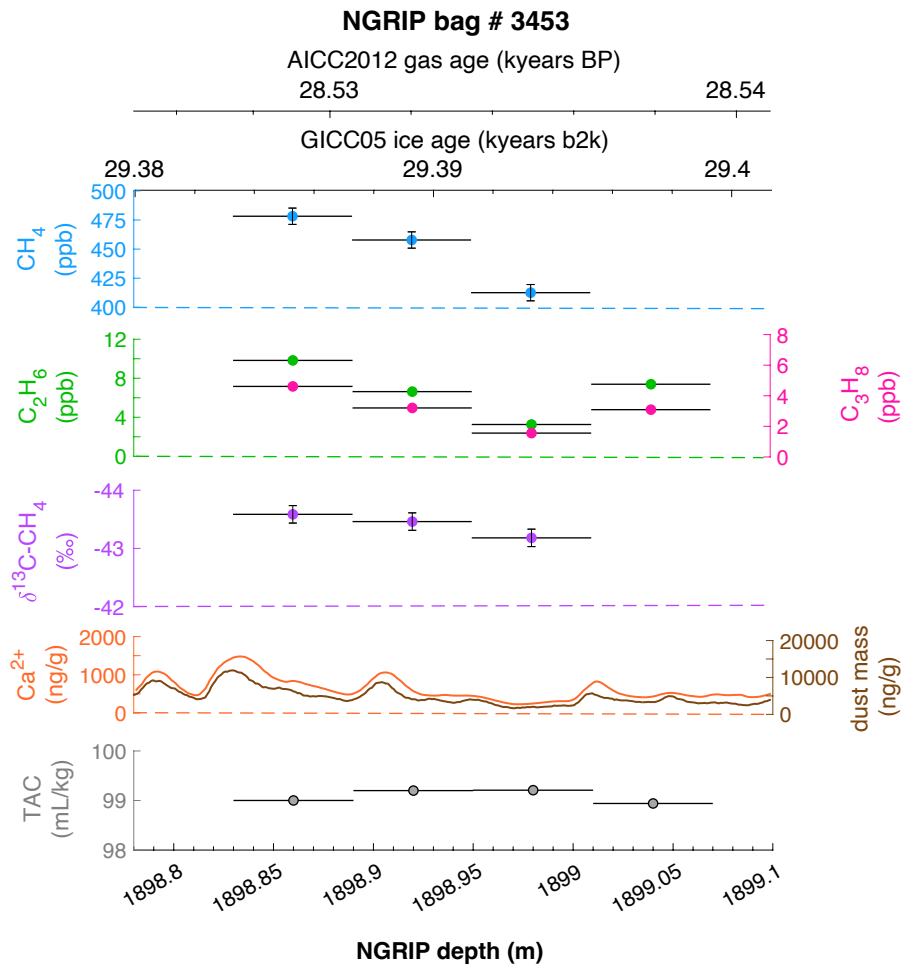


1238

1239 **Figure A1: Detailed data overview for the neighbouring NGRIP bags 3331 & 3332.** Bag-specific overview of
1240 several parameters measured for each sample in this bag: methane, ethane, propane, Ca^{2+} , mineral dust mass, TAC
1241 (Total Air Content), $\delta^{13}\text{C-CH}_4$, indicated at the NGRIP depth (bottom axis) and the AICC2012 gas age (upper top
1242 axis) and the GICC05 ice age (lower top axis). The mineral dust record is taken from Ruth et al. (2003), the Ca^{2+}
1243 record from Erhardt et al. (2022).

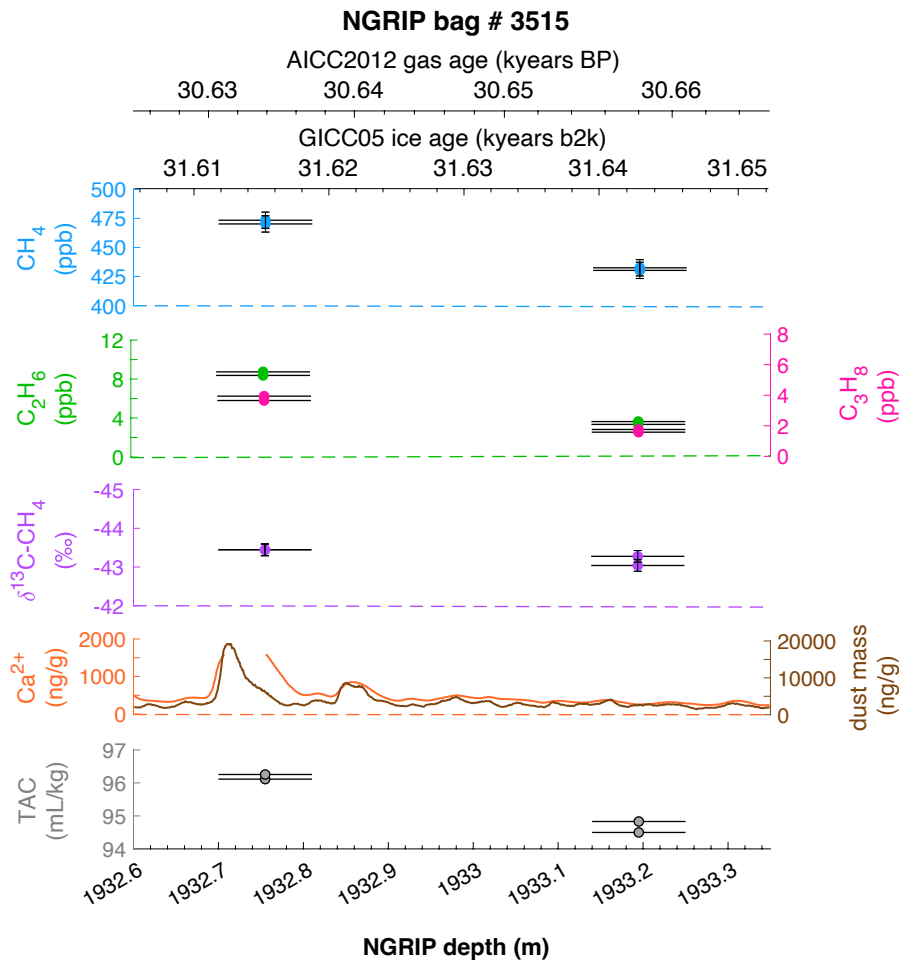
1244

1245



1246
1247
1248
1249
1250
1251
1252
1253
1254
1255

Figure A2: **Detailed data overview for NGRIP bag 3453.** Bag-specific overview of parameters measured for each sample in this bag: methane, ethane, propane, Ca^{2+} , mineral dust mass, TAC (Total Air Content), $\delta^{13}\text{C-CH}_4$, indicated at the NGRIP depth (bottom axis) and the AICC2012 gas age (upper top axis) and the GICC05 ice age (lower top axis). The mineral dust record is taken from Ruth et al. (2003), the Ca^{2+} record from Erhardt et al. (2022).

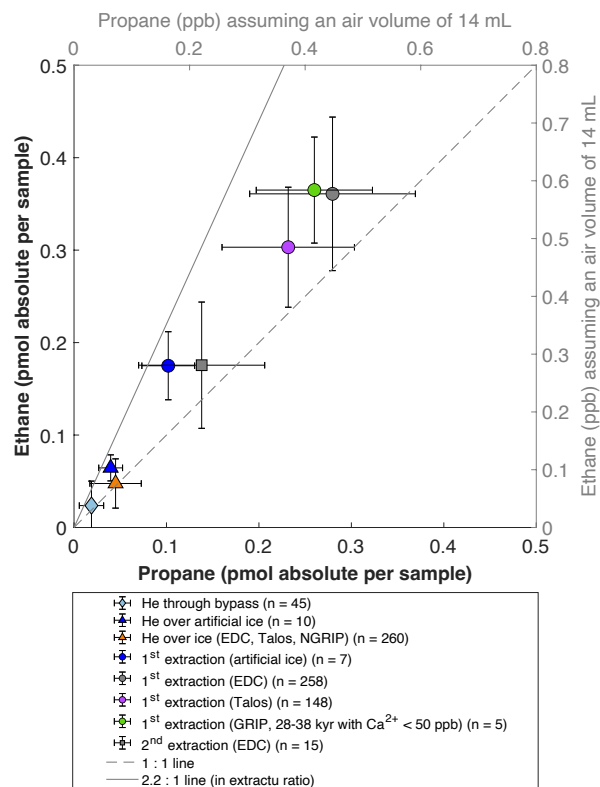


1256
1257
1258
1259
1260
1261
1262
1263
1264
1265
1266
1267
1268
1269
1270
1271
1272
1273
1274
1275
1276
1277

Figure A3: **Detailed data overview for NGRIP bag 3515.** Bag-specific overview of parameters measured for each sample in this bag: methane, ethane, propane, Ca²⁺, mineral dust mass, TAC (Total Air Content), δ¹³C-CH₄, indicated at the NGRIP depth (bottom axis) and the AICC2012 gas age (upper top axis) and the GICC05 ice age (lower top axis). The mineral dust record is taken from Ruth et al. (2003), the Ca²⁺ record from Erhardt et al. (2022). Note that there is a gap in the Ca²⁺ record which was corrected by a fill routine for the analysis of the two measured samples at this depth.

1278 **Appendix B**

1279



1280

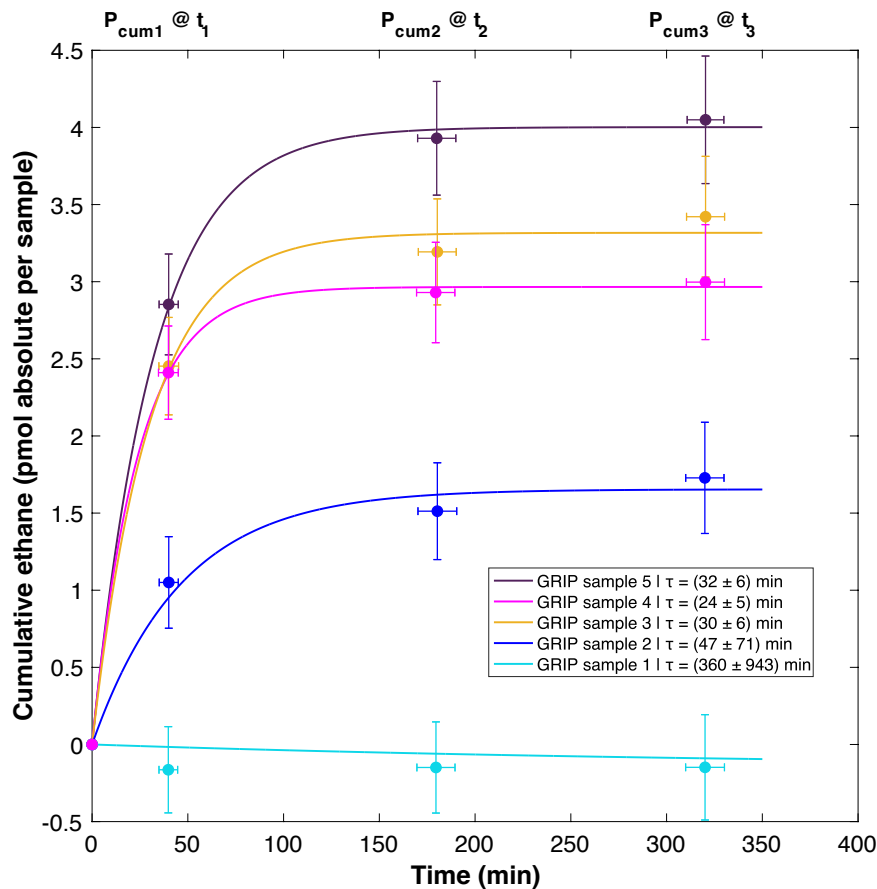
1281 **Figure B1: Collection of different measurement modes and ice core sample locations to estimate individual**
 1282 **blank contributions.** The mode “He through bypass” (diamond) refers to a measurement type where helium is
 1283 injected into our system but without flowing through our extraction vessel. “He over ice” (triangles) refers to
 1284 helium injections over the unmelted ice core sample. Results from the 1st extraction are shown for different ice
 1285 cores (artificial gas-free ice, Talos Dome, EDC, GRIP; colored circles). The 2nd extraction of the Antarctic EDC
 1286 ice core is marked as grey square. Lines with ethane/propane ratios are for orientation only.

1287

1288 In this section we provide background information of how we determined the blank
 1289 contributions for our alkane measurements for the different measurement modes. Overall, our
 1290 strategy is similar to the measurements which were published earlier in 2014 (Schmitt et al.,
 1291 2014). Here we include more measurements performed since then with our $\delta^{13}\text{C}\text{-CH}_4$ device.
 1292 Following the classic usage, blank contributions are related to the measurement device itself
 1293 rather than to the sample, thus we report the measured values of the species as absolute amount
 1294 in pmol with respect to a measurement procedure (sample run). To compare these absolute
 1295 values with the classic units of species concentration in the air for an ice sample in ppb, Fig.
 1296 B1 has secondary axes (grey) for the species concentrations in ppb for an assumed sample size
 1297 of air of 14 mL STP (our typical ice core sample size).

1298 Since our extraction device is at vacuum conditions, a blank contribution from leaks that allow
 1299 ambient air with relatively high ethane and propane concentrations to be collected together with
 1300 our sample seems the most straightforward risk. To quantify this leak contribution, we routinely

1301 perform so called “He over ice” runs where a helium flow is passed over the unmelted ice core
1302 sample and the species are trapped on the cold activated carbon trap (see details in Schmitt et
1303 al., 2014). The trapping duration is the same as for the 1st extraction, thus this “He over ice”
1304 run mimics the contribution for the 1st extraction. As can be seen in Fig. B1, for ethane this
1305 “leak contribution” is typically <0.1 ppb, thus small compared to concentrations we see for
1306 dust-rich Greenland ice samples with about 6 ppb (see Fig. 5). However, this “He over ice”
1307 does not capture the actual melting process of the ice sample and represents the lowest blank
1308 boundary for our ice core samples. To mimic the full procedure an ice core samples experiences,
1309 we run a limited number of artificial gas-free ice samples (blue circles in Fig. B1). The ethane
1310 values obtained for these artificial ice sample is around 0.3 ppb and thus considerably higher
1311 than for the procedure without melting. This indicates that the presence of liquid water may
1312 lead to a desorption or production of alkanes from the inner walls of our extraction vessel.
1313 Alternatively, our artificial ice still contains traces of alkanes. So far, we could not solve this
1314 issue and more experiments are needed. A much larger data set on the upper boundary of the
1315 extraction blank comes from routine measurements of Antarctic ice core samples with the
1316 primary target of stable isotope analyses of CH₄ and N₂O. These Antarctic samples cover glacial
1317 and interglacial time intervals and the measured ethane values are typically around 0.55 ppb.
1318 Since the reconstructed atmospheric background for ethane in Antarctic ice is lower with values
1319 in the range of 0.1 – 0.15 ppb for the late Holocene (Nicewonger et al., 2018), a realistic blank
1320 contribution for our 1st extraction is on the order of 0.4 to 0.5 ppb. An additional constraint
1321 comes from five stadial GRIP samples from the time interval 28-38 kyears (green circle in Fig.
1322 B1) that have very low Ca²⁺ content (< 50 ppb) and thus have likely a negligible contribution
1323 from a dust-related *in extractu* component. The measured ethane concentration from these
1324 GRIP samples is very similar to the Antarctic ice core samples. One possible explanation would
1325 be that the atmospheric ethane concentration during the glacial was similar and low for both
1326 hemispheres. Regardless of the individual contributions, for our considerations of dust-related
1327 *in extractu* production in Greenland ice cores the upper estimate for the sum of atmospheric
1328 background and blank contribution is about 0.55 ppb (about 0.35 pmol) for ethane. Since the
1329 ethane to propane ratio for these non-dust contributions is about 1.5, the corresponding propane
1330 values are lower by that value. Importantly, since the ethane to propane ratio for our dust-related
1331 production is with 2.2 rather similar, its impact on the calculated ethane to propane ratio (e.g.
1332 Fig. 4) is very minor and small within the error estimate. For that reason, we did not correct our
1333 Greenland measurements for any blank contribution and showed the values as measured along
1334 with measurements of Antarctic ice cores samples which serve as first-order blank estimates.



1339 Figure C1: **Temporal dynamics of excess ethane production in GRIP ice core samples.** Cumulative ethane
 1340 amount from the 1st, 2nd, and 3rd extraction in relation to the time available for a potential reaction in the meltwater
 1341 during each extraction. We assume a first-order reaction kinetic as model for our observations where the mean
 1342 half-life time (τ) and standard deviations are calculated for each GRIP sample from the compilation of all 1000
 1343 iterations of our Monte Carlo approach. The numbered samples can also be found in Fig. 7a.
 1344

1345 The general equation to describe a first-order chemical reaction or exponential decay process
 1346 (e.g. release of adsorbed gas from the adsorbent) is Eqn. (1).

$$1348 \quad N(t) = N_0 \cdot e^{-(t/\tau)} \quad (1)$$

1350 With N_0 being the total amount of substance (reactant) at the start of the reaction. $N(t)$ equals
 1351 the remaining amount of the reactant at time t , and t being time of reaction and τ , the mean
 1352 lifetime of the reaction. In our case, we cannot determine $N(t)$ neither do we know N_0 but we
 1353 experimentally determined the cumulative amount of the product, $P_{\text{cum}(t)}$, at three different times
 1354 as our observable quantity. Thus, in Eqn. 2 we define $P_{\text{cum}(t)}$ as the difference between N_0 and
 1355 $N(t)$.

1356

1357
$$P_{\text{cum}(t)} = N_0 - N(t) \quad (2)$$

1358

1359 Replacing $N(t)$ in Eqn. 1 with our definition in Eqn. 2 we obtain Eqn. 3, which contains two fit
1360 parameters, N_0 and τ , as well as our observable parameter $P_{\text{cum}(t)}$, i.e. the cumulative amount of
1361 alkane for a certain time step.

1362

1363
$$P_{\text{cum}(t)} = N_0 - N_0 * e^{-t/\tau} \quad (3)$$

1364

1365 For the five GRIP samples we have three consecutive measurements each, the 1st, 2nd, and 3rd
1366 extraction. The time-dependent $P_{\text{cum}(t)}$ values are as follows: $P_{\text{cum}0}$ is defined as 0, representing
1367 the state of the unmelted ice sample before liquid water is present. $P_{\text{cum}1}$ is the measured amount
1368 from the 1st extraction (ice extraction) minus the estimated contribution from the atmosphere
1369 and minus the blank contribution for the 1st extraction. $P_{\text{cum}2}$ is the sum of $P_{\text{cum}1}$ and the value
1370 from the 2nd extraction minus the blank contribution of the 2nd extraction. Similarly, $P_{\text{cum}3}$ is the
1371 sum of $P_{\text{cum}2}$ and the value from the 3rd extraction minus the blank for the 3rd extraction.

1372 To account for the uncertainties of the involved measurements and corrections, we added
1373 normally distributed errors to the following parameters (measured value $\pm 5\%$; blank $\pm 20\%$;
1374 atmospheric contribution $\pm 50\%$), and we also assigned an uncertainty of 5 min to the time to
1375 account for variations of the melting speed of the ice and delays between the individual
1376 measurements (1st, 2nd, 3rd).

1377 For the fitting procedure we used the Matlab built in nonlinear least-squares solver called
1378 'lsqcurvefit' and performed 1000 runs where we varied the above-mentioned input parameters.
1379 The output of the function are the two fit parameters, i.e., N_0 and τ . From the 1000 runs we
1380 calculated the mean and the 1 sigma standard deviation of the lifetime.

1381

1382 Note, this approach can only be suitably applied to ethane and propane as the past atmospheric
1383 contribution for these gases in the 1st extraction is typically small against the excess contribution
1384 for dust-rich samples. For our five GRIP samples, where we have three consecutive extractions,
1385 four samples are considered "dust-rich" and are suitable to provide robust estimates for τ . In
1386 contrast, one sample is from an interstadial period with very low dust content and thus shows
1387 negligible production of alkanes in all three extractions. While this sample is not suited to
1388 provide robust estimates for τ , this sample allows to assess the first-order plausibility of the
1389 blank correction and the assumed atmospheric background for ethane for the 1st extraction

1390 (sample number 1, bottom-most sample). For a sample without any *in extractu* production, the
1391 cumulative curve should be flat at around 0 which is the case within our error estimates.

1392

1393

1394

1395 **Code availability**

1396 No special code related to the manuscript.

1397

1398 **Data availability**

1399 Data is provided on request to the authors.

1400

1401 **Author contribution**

1402 The experimental approach was defined by JS, HF and MM. MM and BS performed the
1403 measurements; MM and JS analyzed the data; MM wrote the manuscript draft; MM prepared
1404 the manuscript with contributions from all co-authors.

1405

1406 **Competing interests**

1407 The authors declare that they have no conflict of interest.

1408

1409 **Disclaimer**

1410 None.

1411

1412 **Special issue statement**

1413 Ice core science at the three poles (CP/TC inter-journal SI)

1414

1415 **Acknowledgments**

1416 We thank Murat Aydin for very helpful review comments. The research leading to these results
1417 has received funding from the Swiss National Science Foundation (no. 200020_172506 &
1418 200020B_200328). This work is a contribution to the NorthGRIP ice core project, which is
1419 directed and organized by the Department of Geophysics at the Niels Bohr Institute for
1420 Astronomy, Physics and Geophysics, University of Copenhagen. It is supported by funding
1421 agencies in Denmark (SNF), Belgium (FNRS-CFB), France (IFRTP and NSU/CNRS),
1422 Germany (AWI), Iceland (RannIs), Japan (MEXT), Sweden (SPRS), Switzerland (SNF), and
1423 the United States (NSF).

1424 **References**

1425

1426 Althoff, F., Jugold, A. and Keppler, F.: Methane formation by oxidation of ascorbic acid
1427 using iron minerals and hydrogen peroxide. *Chemosphere* 80, 286–292,
1428 <https://doi.org/10.1016/j.chemosphere.2010.04.004>, 2010

1429

1430 Althoff, F., Benzing, K., Comba, P., McRoberts, C., Boyd, D. R., Greiner, S. and Keppler, F.:
1431 Abiotic methanogenesis from organosulphur compounds under ambient conditions, *Nat*
1432 *Commun*, 5, 4205, <https://doi.org/10.1038/ncomms5205>, 2014

1433

1434 Anklin, M., Barnola, J.-M., Schwander, J., Stauffer, B., and Raynaud, D.: Processes affecting
1435 the CO₂ concentrations measured in Greenland ice, *Tellus*, 47, 461-470,
1436 <https://doi.org/10.1034/j.1600-0889.47.issue4.6.x>, 1995

1437

1438 Apel, K. and Hirt, H.: Reactive Oxygen Species: Metabolism, Oxidative Stress, and Signal
1439 Transduction, *Annual Review of Plant Biology* 2004, 55:1, 373-399,
1440 <https://doi.org/10.1146/annurev.arplant.55.031903.141701>, 2004

1441

1442 Austin, A. T., Méndez, M. S., and Ballaré, C. L.: Photodegradation alleviates the lignin
1443 bottleneck for carbon turnover in terrestrial ecosystems, *PNAS*, 13 (16), 4392-4397,
1444 <https://doi.org/10.1073/pnas.1516157113>, 2016

1445

1446 Baumgartner, M., Schilt, A., Eicher, O., Schmitt, J., Schwander, J., Spahni, R., Fischer, H.,
1447 and Stocker, T. F.: High-resolution inter-polar difference of atmospheric methane around the
1448 Last Glacial Maximum, *Biogeosciences*, 9, 3961–3977, [https://doi.org/10.5194/bg-9-3961-](https://doi.org/10.5194/bg-9-3961-2012)
1449 2012, 2012

1450

1451 Baumgartner, M., Kindler, P., Eicher, O., Floch, G., Schilt, A., Schwander, J., Spahni, R.,
1452 Capron, E., Chappellaz, J., Leuenberger, M., Fischer, H., and Stocker, T. F.: NGRIP
1453 CH₄ concentration from 120 to 10 kyr before present and its relation to a δ¹⁵N temperature
1454 reconstruction from the same ice core, *Clim. Past*, 10, 903–920, [https://doi.org/10.5194/cp-](https://doi.org/10.5194/cp-10-903-2014)
1455 10-903-2014, 2014

1456

1457 Beck, J., Bock, M., Schmitt, J., Seth, B., Blunier, T., and Fischer, H.: Bipolar carbon and
1458 hydrogen isotope constraints on the Holocene methane budget, *Biogeosciences*, 15, 7155–
1459 7175, <https://doi.org/10.5194/bg-15-7155-2018>, 2018

1460

1461 Bernard, B., Brooks, J.M. and Sackett, W.M.: A geochemical model for characterization of
1462 hydrocarbon gas sources in marine sediments. In: 9th Annual Offshore Technology
1463 Conference, Houston, Texas, May 1977, 435–438 (OTC 2934), [https://doi.org/10.4043/2934-](https://doi.org/10.4043/2934-MS)
1464 MS, 1977

1465

1466 Biscaye, P. E., Grousset, F. E., Revel, M., Van der Gaast, S., Zielinski, G. A., Vaars, A. and
1467 G. Kukla: Asian provenance of Glacial dust (stage 2) in the Greenland Ice Sheet Project 2 Ice
1468 Core, Summit, Greenland, *J. Geophys. Res.*, 102, 26,765-26,781, 1997

1469

1470 Bock, M., Schmitt, J., Behrens, M., Möller, L., Schneider, R., Sapart, C. and Fischer, H.: A
1471 gas chromatography/pyrolysis/isotope ratio mass spectrometry system for high- precision dD
1472 measurements of atmospheric methane extracted from ice cores, *Rapid Commun. Mass*
1473 *Spectrom*, 24, 621–633, <https://doi.org/10.1002/rcm.4429>, 2010a

1474

1475 Bock, M., Schmitt, J., Blunier, T., Fischer, H., Möller, L. and Spahni, R.: Hydrogen
1476 Isotopes Preclude Marine Hydrate CH₄ Emissions at the Onset of Dansgaard- Oeschger
1477 Events, *Science*, 328, 1686-1689, <https://doi.org/10.1126/science.1187651>, 2010b
1478

1479 Bock, M., Schmitt, J., Beck, J., Schneider, R., and Fischer, H.: Improving accuracy and
1480 precision of ice core δD(CH₄) analyses using methane pre-pyrolysis and hydrogen post-
1481 pyrolysis trapping and subsequent chromatographic separation, *Atmos. Meas. Tech.*, 7, 1999–
1482 2012, <https://doi.org/10.5194/amt-7-1999-2014>, 2014
1483

1484 Bock, M., Schmitt, J., Beck, J., Seth, B., Chappellaz, J. and Fischer, H.: Glacial/ interglacial
1485 wetland, biomass burning, and geologic methane emissions constrained by dual stable
1486 isotopic CH₄ ice core records, *PNAS*, 114 (29), E5778-E5786,
1487 <https://doi.org/10.1073/pnas.1613883114>, 2017
1488

1489 Bruhn, D., Mikkelsen, T. N., Øbro, J., Willats, W. G. T. and Ambus, P.: Effects of
1490 temperature, ultraviolet radiation and pectin methyl esterase on aerobic methane release from
1491 plant material, *Plant Biology*, 11, 43-48, <https://doi.org/10.1111/j.1438-8677.2009.00202.x>,
1492 2009
1493

1494 Campen, R. K., Sowers, T., and Alley, R. B.: Evidence of microbial consortia metabolizing
1495 within a low-latitude mountain glacier, *Geology*, 31, 231–234, [https://doi.org/10.1130/0091-7613\(2003\)031<0231:EOMCMW>2.0.CO;2](https://doi.org/10.1130/0091-7613(2003)031<0231:EOMCMW>2.0.CO;2), 2003
1496
1497

1498 Chappellaz, J., Blunier, T., Kints, S., Dällenbach, A., Barnola, J. M., Schwander, J., Raynaud,
1499 D. and Stauffer B.: Changes in the atmospheric CH₄ gradient between Greenland and
1500 Antarctica during the Holocene, *Geophys. Res. Lett.*, Volume 102, 15987-15997,
1501 <https://doi.org/10.1029/97JD01017>, 1997
1502

1503 Cheng, A. L. and Huang, W. L.: Selective adsorption of hydrocarbon gases on clays and
1504 organic matter, *Org. Geochem.*, 35, 413-423,
1505 <https://doi.org/10.1016/j.orggeochem.2004.01.007>, 2004
1506

1507 Dan, J., Kumai, T., Sugimoto, A. and Murase, J.: Biotic and abiotic methane releases from
1508 Lake Biwa sediment slurry, *Limnology* 5, 149–154, <https://doi.org/10.1007/s10201-004-0124-7>, 2004
1509
1510

1511 Derendorp, L., Holzinger, R., Wishkerman, A., Keppler, F., and Röckmann, T.: VOC
1512 emissions from dry leaf litter and their dependence on temperature, *Biogeosciences Discuss.*,
1513 7, 823–854, <https://doi.org/10.5194/bgd-7-823-2010>, 2010
1514

1515 Derendorp, L., Holzinger, R., Wishkerman, A., Keppler, F., and Röckmann, T.: Methyl
1516 chloride and C₂-C₅ hydrocarbon emissions from dry leaf litter and their dependence on
1517 temperature, *Atmospheric Environment*, 45, 3112-3119,
1518 <https://doi.org/10.1016/j.atmosenv.2011.03.016>, 2011
1519

1520 Dumelin, E.E. and Tappel, A.L.: Hydrocarbon gases produced during in vitro peroxidation of
1521 polyunsaturated fatty acids and decomposition of preformed hydroperoxides, *Lipids*, 12, 894,
1522 <https://doi.org/10.1007/BF02533308>, 1977
1523

1524 Dyonisius, M. N., Petrenko, V. V., Smith, A.M., Hua, Q., Yang, B., Schmitt, J., Beck, J.,
1525 Seth, B., Bock, M., Hmiel, B., Vimont, I., Menking, J. A., Shackleton, S. A., Baggenstos, D.,

1526 Bauska, T. K., Rhodes, R., Sperlich, P., Beaudette, R., Harth, C., Kalk, M., Brook, E. J.,
1527 Fischer, H., Severinghaus, J. P. and Weiss, R. F.: Old carbon reservoirs were not important in
1528 the deglacial methane budget, *Science*, 367(6480), 907-910,
1529 <https://doi.org/10.1126/science.aax0504>, 2020
1530
1531 Erhardt, T., Bigler, M., Federer, U., Gfeller, G., Leuenberger, D., Stowasser, O.,
1532 Röthlisberger, R., Schüpbach, S., Ruth, U., Twarloh, B., Wegner, A., Goto-Azuma, K.,
1533 Kuramoto, T., Kjær, H. A., Vallelonga, P. T., Siggaard-Andersen, M.-L., Hansson, M. E.,
1534 Benton, A. K., Fleet, L. G., Mulvaney, R., Thomas, E. R., Abram, N., Stocker, T. F., and
1535 Fischer, H.: High resolution aerosol concentration data from the Greenland NorthGRIP and
1536 NEEM deep ice cores, *Earth Syst. Sci. Data Discuss.*, 14, 1215–1231,
1537 <https://doi.org/10.5194/essd-14-1215>, 2022
1538
1539 Etiope, G. and Klusman, R. W.: Geologic emissions of methane to the atmosphere,
1540 *Chemosphere*, 49, 8, 777-789, [https://doi.org/10.1016/S0045-6535\(02\)00380-6](https://doi.org/10.1016/S0045-6535(02)00380-6), 2002
1541
1542 Etiope G., Martinelli G., Caracausi, A. and Italiano, F.: Methane seeps and mud volcanoes in
1543 Italy: gas origin, fractionation and emission to the atmosphere, *Geophys. Res. Lett.*, 34,
1544 <https://doi.org/10.1029/2007GL030341>, 2007
1545
1546 Etiope G., Lassey K. R., Klusman R. W. and Boschi, E.: Reappraisal of the fossil methane
1547 budget and related emission from geologic sources, *Geophys. Res. Lett.*, 35,
1548 <https://doi.org/10.1029/2008GL033623>, 2008
1549
1550 Frahry, G. and Schopfer, P.: Hydrogen peroxide production by roots and its stimulation by
1551 exogenous NADH, *Physiologia Plantarum*, 103, 395-404, <https://doi.org/10.1034/j.1399-3054.1998.1030313.x>, 1998
1552
1553
1554 Flückiger J., Blunier T., Stauffer B., Chappellaz M., Spahni R., Kawamura K., Schwander J.,
1555 Stocker T. F. and Dahl-Jensen D.: N₂O and CH₄ variations during the last glacial epoch:
1556 Insight into global processes, *Global Biogeochem. Cy* 18, 1020,
1557 <https://doi.org/10.1029/2003GB002122>, 2004
1558
1559 Fuhrer, K. and Legrand, M.: Continental biogenic species in the Greenland Ice Core Project
1560 ice core: Tracing back the biomass history of the North American continent, *J. Geophys. Res.*,
1561 102(C12), 26735– 26745, <https://doi.org/10.1029/97JC01299>, 1997
1562
1563 Georgiou, C. D., Sun, H. J., McKay, C. P., Grintzalis, K., Papapostolou, I., Zisimopoulos, D.,
1564 Panagiotidis, K., Zhang, G., Koutsopoulou, E., Christidis, G. E. and Margiolaki, I.: Evidence
1565 for photochemical production of reactive oxygen species in desert soils, *Nat.*
1566 *Commun.*, 6, 7100, <https://doi.org/10.1038/ncomms8100>, 2015
1567
1568 Giorio, C., Kehrwald, N., Barbante, C., Kalberer, M., King, A. C. F., Thomas, E. R., Wolff,
1569 E. W. and Zennaro, P.: Prospects for reconstructing paleoenvironmental conditions from
1570 organic compounds in polar snow and ice, *Quaternary Science Reviews*, 183, 1-22,
1571 <https://doi.org/10.1016/j.quascirev.2018.01.007>, 2018
1572
1573 Gu, Q., Chang, S. X., Wang, Z. P., Feng, J. C., Chen, Q. S. and Han, X. G.: Microbial versus
1574 non-microbial methane releases from fresh soils at different temperatures, *Geoderma*, 284,
1575 178-184, <https://doi.org/10.1016/j.geoderma.2016.08.027>, 2016
1576

1577 Han, C., Do Hur, S., Han, Y., Lee, K., Hong, S., Erhard, T., Fischer, H., Svensson, A. M.,
1578 Steffensen, J. P. and Vallelonga, P.: High-resolution isotopic evidence for a potential Saharan
1579 provenance of Greenland glacial dust. *Sci Rep* 8, 15582, [https://doi.org/10.1038/s41598-018-](https://doi.org/10.1038/s41598-018-33859-0)
1580 33859-0, 2018

1581
1582 Harris, E., Sinha, B., van Pinxteren, D., Tilgner, A., Wadinga Fomba, K., Schneider, J., Roth,
1583 A., Gnauk, T., Fahlbusch, B., Mertes, S., Lee, T., Collett, J., Foley, S., Borrmann, S., Hoppe,
1584 P. and Herrmann, H.: Enhanced Role of Transition Metal Ion Catalysis During In-Cloud
1585 Oxidation of SO₂, *Science*, 340, 727-730, <https://doi.org/doi:10.1126/science.1230911>, 2013
1586

1587 Helmig, D., Petrenko, V., Martinerie, P., Witrant, E., Röckmann, T., Zuiderweg, A.,
1588 Holzinger, R., Hueber, J., Thompson, C., White, J. W. C., Sturges, W., Baker, A., Blunier, T.,
1589 Etheridge, D., Rubino, M., and Tans, P.: Reconstruction of Northern Hemisphere 1950–2010
1590 atmospheric non-methane hydrocarbons, *Atmos. Chem. Phys.*, 14, 1463-1483,
1591 <https://doi.org/10.5194/acp-14-1463>, 2014
1592

1593 Hoheisel, A., Yeman, C., Dinger, F., Eckhardt, H., and Schmidt, M.: An improved method for
1594 mobile characterisation of $\delta^{13}\text{C}_{\text{CH}_4}$ source signatures and its application in Germany, *Atmos.*
1595 *Meas. Tech.*, 12, 1123–1139, <https://doi.org/10.5194/amt-12-1123-2019>, 2019.
1596

1597 Hurkuck, M., Althoff, F., Jungkunst, H. F., Jugold, A. and Keppler, F.: Release of methane
1598 from aerobic soil: An indication of a novel chemical natural process?, *Chemosphere*, 86, 684-
1599 689, <https://doi.org/10.1016/j.chemosphere.2011.11.024>, 2012
1600

1601 Ji L., Zhang T., Milliken K. L., Qu J. and Zhang X.: Experimental investigation of main
1602 controls to methane adsorption in clay-rich rocks, *Appl. Geochem.* 27, 2533–2545,
1603 <https://doi.org/10.1016/j.apgeochem.2012.08.027>, 2012
1604

1605 John, W. W. and Curtis, R. W.: Isolation and Identification of the Precursor of Ethane
1606 in *Phaseolus vulgaris* L., *Plant Physiology*, 59, 521–522, <https://doi.org/10.1104/pp.59.3.521>,
1607 1977
1608

1609 Jugold, A., Althoff, F., Hurkuck, M., Greule, M., Lenhart, K., Lelieveld, J., and Keppler, F.:
1610 Non-microbial methane formation in oxic soils, *Biogeosciences*, 9, 5291–5301,
1611 <https://doi.org/10.5194/bg-9-5291-2012>, 2012
1612

1613 Katagi, T.: Photoinduced Oxidation of the organophosphorus Fungicide Tolclofs-methyl on
1614 Clay Minerals, *J. Agric. Food Cham.*, 38, 1595-1600, 1990
1615

1616 Kaufmann, P. R., Federer, U., Hutterli, M. A., Bigler, M., Schüpbach, S., Ruth, U., Schmitt, J.
1617 and Stocker, T. F.: An Improved Continuous Flow Analysis System for High-Resolution
1618 Field Measurements on Ice Cores, *Environmental Science & Technology*, 42 (21), 8044-
1619 8050, <https://doi.org/10.1021/es8007722>, 2008
1620

1621 Keeling, C. D.: The concentration and isotopic abundance of carbon dioxide in rural areas,
1622 *Geochim. Cosmochim. Acta*, 13, 322–334 [https://doi.org/10.1016/0016-7037\(58\)90033-](https://doi.org/10.1016/0016-7037(58)90033-4)
1623 4.1958, 1958
1624

1625 Keeling, C. D.: The concentration and isotopic abundance of carbon dioxide in rural and
1626 marine air, *Geochim. Cosmochim. Acta*, 24, 277–298, [https://doi.org/10.1016/0016-](https://doi.org/10.1016/0016-7037(61)90023-0)
1627 7037(61)90023-0, 1961

1628
1629 Keppler, F., Hamilton, J. T. G., Braß, M. and Röckmann, T.: Methane emissions from
1630 terrestrial plants under aerobic conditions, *Nature* 439, 187–191,
1631 <https://doi.org/10.1038/nature04420>, 2006
1632
1633 Keppler, F., Hamilton, J. T. G., McRoberts, W. C., Vigano, I., Braß, M. and Röckmann, T.:
1634 Methoxyl groups of plant pectin as a precursor of atmospheric methane: evidence from
1635 deuterium labelling studies, *New Phytologist*, 178, 808-814, <https://doi.org/10.1111/j.1469-8137.2008.02411.x>, 2008
1636
1637 Kibanova, D., Trejo, M., Destailats, H. and Cervini-Silva, J.: Photocatalytic activity of
1638 kaolinite, *Catalysis Communications*, 12, 698-702,
1639 <https://doi.org/10.1016/j.catcom.2010.10.029>, 2011
1640
1641 Köhler, P., Fischer, H., Schmitt, J., and Munhoven, G.: On the application and interpretation
1642 of Keeling plots in paleo climate research – deciphering $\delta^{13}\text{C}$ of atmospheric CO_2 measured in
1643 ice cores, *Biogeosciences*, 3, 539–556, <https://doi.org/10.5194/bg-3-539-2006>, 2006
1644
1645 Lee, L. E., Edwards, J. S., Schmitt, J., Fischer, H., Bock, M. and Brook, E. J.: Excess methane
1646 in Greenland ice cores associated with high dust concentrations, *Geochim. Cosmochim. Acta*,
1647 270, 409-430, <https://doi.org/10.1016/j.gca.2019.11.020>, 2020
1648
1649 Legrand, M., and Delmas, R.: Soluble Impurities in Four Antarctic Ice Cores Over the Last
1650 30000 Years, *Annals of Glaciology*, 10, 116-120,
1651 <https://doi.org/10.3189/S0260305500004274>, 1988
1652
1653 Liu, J., Chen, H., Zhu, Q., Shen, Y., Wang, X., Wang, M., Peng, C.: A novel pathway of
1654 direct methane production and emission by eukaryotes including plants, animals and fungi:
1655 An overview, *Atmospheric Environment*, 115, 26,
1656 <https://doi.org/10.1016/j.atmosenv.2015.05.019>, 2015
1657
1658 Liu, D., Yuan, P., Liu, H., Li, T., Tan, D., Yuan, W., He, H.: High-pressure adsorption of
1659 methane on montmorillonite, kaolinite and illite, *Applied Clay Science*, 85, 25-30,
1660 <https://doi.org/10.1016/j.clay.2013.09.009>, 2013
1661
1662 Lupker, M., Aciego, S. M., Bourdon, B., Schwander, J., and Stocker, T. F.: Isotopic tracing
1663 (Sr, Nd, U and Hf) of continental and marine aerosols in an 18th century section of the Dye-3
1664 ice core (Greenland), *Earth Pla Sci Let*, 295, 277-286,
1665 <https://doi.org/10.1016/j.epsl.2010.04.010>, 2010
1666
1667 McLeod, A. R., Newsham, K. K. and Fry, S.C.: Elevated UV-B radiation modifies the
1668 extractability of carbohydrates from leaf litter of *Quercus robur*, *Soil Biology and*
1669 *Biochemistry*, 39, Issue 1, 116-126, <https://doi.org/10.1016/j.soilbio.2006.06.019>, 2007
1670
1671 McLeod, A.R., Fry, S.C., Loake, G.J., Messenger, D.J., Reay, D.S., Smith, K.A. and Yun, B.-
1672 W.: Ultraviolet radiation drives methane emissions from terrestrial plant pectins, *New*
1673 *Phytologist*, 180, 124-132, <https://doi.org/10.1111/j.1469-8137.2008.02571.x>, 2008
1674
1675 Messenger, D.J., McLeod, A. R. and Fry, S.C.: The role of ultraviolet radiation,
1676 photosensitizers, reactive oxygen species and ester groups in mechanisms of methane
1677

1678 formation from pectin, *Plant, Cell & Environment*, 32: 1-9, [https://doi.org/10.1111/j.1365-](https://doi.org/10.1111/j.1365-3040.2008.01892.x)
1679 3040.2008.01892.x, 2009
1680
1681 Milkov, A. V. and Etiope, G.: Revised genetic diagrams for natural gases based on a global
1682 dataset of >20,000 samples, *Organic Geochemistry*, 125, 109-120,
1683 <https://doi.org/10.1016/j.orggeochem.2018.09.002>, 2018
1684
1685 Mitchell, L., Brook, E., Lee, J. E., Buizert, C., and Sowers, T.: Constraints on the Late
1686 Holocene anthropogenic contribution to the atmospheric methane budget, *Science* 342, 964–
1687 966, <https://doi.org/10.1126/science.1238920>, 2013
1688
1689 Miteva V., Teacher C., Sowers T. and Brenchley, J.: Comparison of the microbial diversity at
1690 different depths of the GISP2 Greenland ice core in relationship to deposition climates,
1691 *Environ. Microbiol.*, 11, 640–656, <https://doi.org/10.1111/j.1462-2920.2008.01835.x>, 2009
1692
1693 Möller, L., Sowers, T., Bock, M., Spahni, R., Behrens, M., Schmitt, J., Miller, H. and Fischer,
1694 H.: Independent variations of CH₄ emissions and isotopic composition over the past 160,000
1695 years, *Nature Geosci*, 6, 885–890, <https://doi.org/10.1038/ngeo1922>, 2013
1696
1697 Mohnen, D.: Pectin structure and biosynthesis, *Current Opinion in Plant Biology*, 11, 266-
1698 277, <https://doi.org/10.1016/j.pbi.2008.03.006>, 2008
1699
1700 NEEM community members: Eemian interglacial reconstructed from a Greenland folded ice
1701 core, *Nature*, 493, 489–494, <https://doi.org/10.1038/nature11789>, 2013
1702
1703 Nicewonger, M. R., Verhulst, K. R., Aydin, M. and Saltzman, E. S.: Preindustrial
1704 atmospheric ethane levels inferred from polar ice cores: A constraint on the geologic sources
1705 of atmospheric ethane and methane, *Geophys. Res. Lett.*, 43,
1706 <https://doi.org/10.1002/2015GL066854>, 2016
1707
1708 Nicewonger, M. R., Aydin, M., Prather, M. J., and Saltzman, E.S.: Large changes in biomass
1709 burning over the last millennium inferred from paleoatmospheric ethane in polar ice cores,
1710 *Proc. Natl. Acad. Sci. USA*, 115 (49), 12413-12418,
1711 <https://doi.org/10.1073/pnas.1807172115>, 2018
1712
1713 North Greenland Ice Core Project members, High-resolution record of Northern Hemisphere
1714 climate extending into the last interglacial period, *Nature* 431, 147–151,
1715 <https://doi.org/10.1038/nature02805>, 2004
1716
1717 Pires, J., Bestilleiro, M., Pinto, M. and Gil, A.: Selective adsorption of carbon dioxide,
1718 methane and ethane by porous clays heterostructures, *Separation and Purification*
1719 *Technology*, 61, 161-167, <https://doi.org/10.1016/j.seppur.2007.10.007>, 2008
1720
1721 Price, P. B. and Sowers, T.: Temperature dependence of metabolic rates for microbial growth,
1722 maintenance, and survival, *P. Natl. Acad. Sci. USA* 101, 4631–4636,
1723 <https://doi.org/10.1073/pnas.0400522101>, 2004
1724
1725 Rohde, R. A., Price, P. B., Bay, R. C. and Bramall, N. E.: In situ microbial metabolism as a
1726 cause of gas anomalies in ice, *P. Natl. Acad. Sci. USA*, 105, 8667–8672,
1727 <https://doi.org/10.1073/pnas.0803763105>, 2008
1728

1729 Rhodes, R. H., Faïn, X., Stowasser, C., Blunier, T., Chappellaz, C., McConnell, J. R.,
1730 Romanini, D., Mitchell, L. E. and Brook, E. J.: Continuous methane measurements from a
1731 late Holocene Greenland ice core: Atmospheric and in situ signals, *Earth and Planetary
1732 Science Letters*, 368, 9-19, <https://doi.org/10.1016/j.epsl.2013.02.034>, 2013
1733

1734 Rhodes, R. H., Faïn, X., Brook, E. J., McConnell, J. R., Maselli, O. J., Sigl, M., Edwards, J.,
1735 Buizert, C., Blunier, T., Chappellaz, J., and Freitag, J.: Local artifacts in ice core methane
1736 records caused by layered bubble trapping and in situ production: a multi-site investigation,
1737 *Clim. Past*, 12, 1061–1077, <https://doi.org/10.5194/cp-12-1061-2016>, 2016
1738

1739 Ross, D. J. K. and Bustin, R. M.: The importance of shale composition and pore structure
1740 upon gas storage potential of shale gas reservoirs, *Mar. Petrol. Geol.*, 26, 916-927,
1741 <https://doi.org/10.1016/j.marpetgeo.2008.06.004>, 2009
1742

1743 Ruth, U., Wagenbach, D., Steffensen, J. P. and Bigler, M.: Continuous record of microparticle
1744 concentration and size distribution in the central Greenland NGRIP ice core during the last
1745 glacial period, *J. Geophys. Res.*, 108 (D3), 4098, <https://doi.org/10.1029/2002JD002376>,
1746 2003
1747

1748 Ruth, U., Bigler, M., Röthlisberger, R., Siggaard-Andersen, M.-L., Kipfstuhl, S., Goto-
1749 Azuma, K., Hansson, M. E., Johnsen, S. J., Lu, H., and Steffensen, J. P.: Ice core evidence
1750 for a very tight link between North Atlantic and east Asian glacial climate, *Geophys. Res.
1751 Lett.*, 34, L03706, doi:10.1029/2006GL027876, 2007
1752

1753 Schade, G. W., Hofmann, R.-M. and Crutzen, P. J.: CO emissions from degrading plant
1754 matter, *Tellus B: Chemical and Physical Meteorology*, 51:5, 889-908,
1755 <https://doi.org/10.3402/tellusb.v51i5.16501>, 1999
1756

1757 Schilt, A., Baumgartner, M., Blunier, T., Schwander, J., Spahni, R., Fischer, H., and Stocker,
1758 T. F.: Glacial–interglacial and millennial-scale variations in the atmospheric nitrous oxide
1759 concentration during the last 800,000 years, *Quat Sci Rev*, 29, 182-192,
1760 <https://doi.org/10.1016/j.quascirev.2009.03.011>, 2010
1761

1762 Schmitt, J., Seth, B., Bock, M. and Fischer, H.: Online technique for isotope and mixing ratios
1763 of CH₄, N₂O, Xe and mixing ratios of organic trace gases on a single ice core sample, *Atmos.
1764 Meas. Tech.*, 7, 2645–2665, <https://doi.org/10.5194/amt-7-2645-2014>, 2014
1765

1766 Smith, H. J., Wahlen, M., Mastroianni, D., and Taylor, K. C.: The CO₂ concentration of air
1767 trapped in GISP2 ice from the Last Glacial Maximum-Holocene transition, *Geophys Res Lett*,
1768 24, 1-4, <https://doi.org/10.1029/96GL03700>, 1997
1769

1770 Sugimoto, A., Dan, J., Kumai, T. and Murase J.: Adsorption as a methane storage process in
1771 natural lake sediment, *Geophys. Res. Lett.* 30, 2080, <https://doi.org/10.1029/2003GL018162>,
1772 2003
1773

1774 Svensson, A., Biscaye, P. E. and Grousset, F. E.: Characterization of late glacial continental
1775 dust in the Greenland Ice Core Project ice core, *J. Geophys. Res.-Atmos.*, 105, 4637–4656,
1776 <https://doi.org/10.1029/1999JD901093>, 2000
1777

1778 Tian, Y., Yan, C. and Jin, Z.: Characterization of Methane Excess and Absolute Adsorption in
1779 Various Clay Nanopores from Molecular Simulation, *Sci Rep* 7, 12040,
1780 <https://doi.org/10.1038/s41598-017-12123>, 2017
1781

1782 Tung, H. C., Bramall, N. E. and Price, P. B.: Microbial origin of excess methane in glacial ice
1783 and implications for life on Mars, *P. Natl. Acad. Sci. USA* 102, 18292–18296,
1784 <https://doi.org/10.1073/pnas.0507601102>, 2005
1785 Tung, H., Price, P., Bramall, N. and Vrdoljak G.: Microorganisms metabolizing on clay
1786 grains in 3-km-deep Greenland basal ice, *Astrobiology* 6, 69–86.
1787 <https://doi.org/10.1089/ast.2006.6.69>, 2006
1788

1789 Vigano, I., van Weelden, H., Holzinger, R., Keppler, F., McLeod, A., and Röckmann, T.:
1790 Effect of UV radiation and temperature on the emission of methane from plant biomass and
1791 structural components, *Biogeosciences*, 5, 937–947, <https://doi.org/10.5194/bg-5-937-2008>,
1792 2008
1793

1794 Vigano, I., Röckmann, T., Holzinger, R., van Dijk, A., Keppler, F., Greule, M., Brand, W. A.,
1795 Geilmann, H. and van Weelden, H.: The stable isotope signature of methane emitted from
1796 plant material under UV irradiation, *Atmospheric Environment*, 43, 5637-5646,
1797 <https://doi.org/10.1016/j.atmosenv.2009.07.046>, 2009
1798

1799 Vigano, I., Holzinger, R., Keppler, F., Greule, M., Brand, W. A., Geilmann, H., van Weelden,
1800 H. and Röckmann, T.: Water drives the deuterium content of the methane emitted from plants,
1801 *Geochimica et Cosmochimica Acta*, 74, 3865-3873, <https://doi.org/10.1016/j.gca.2010.03.030>,
1802 2010
1803 Wang, Z.P., Han, X.G., Wang, G.G., Song, Y. and Gulledge, J.: Aerobic methane emission
1804 from plants in the Inner Mongolia steppe, *Environmental Science & Technology* 42, 62– 68
1805 <https://doi.org/10.1021/es071224l>, 2008
1806

1807 Wang, Z.P., Xie, Z.Q., Zhang, B.C., Hou, L.Y., Zhou, Y.H., Li, L.H. and Han, X.G.: Aerobic
1808 and Anaerobic Nonmicrobial Methane Emissions from Plant Material, *Environmental Science*
1809 *& Technology* 2011 45 (22), 9531-9537, <https://doi.org/10.1021/es2020132>, 2011
1810

1811 Wang, B., Hou, L., Liu, W. and Wang, Z.: Non-microbial methane emissions from soils,
1812 *Atmospheric Environment*, 80, 290–298, <https://doi.org/10.1016/j.atmosenv.2013.08.010>,
1813 2013
1814

1815 Wang, B., Lerdau, M. and He, Y.: Widespread production of nonmicrobial greenhouse gases
1816 in soils, *Glob Change Biol.*, 23:4472–4482, <https://doi.org/10.1111/gcb.13753>, 2017
1817

1818 Watanabe, M., Watanabe, Y., Kim, Y. S., Koike, T.: Dark aerobic methane emission
1819 associated to leaf factors of two Acacia and five Eucalyptus species, *Atmospheric*
1820 *Environment*, 54, 277-281, <https://doi.org/10.1016/j.atmosenv.2012.02.012>, 2012
1821

1822 Wehr, R. and Saleska, S. R.: The long-solved problem of the best-fit straight line: application
1823 to isotopic mixing lines, *Biogeosciences*, 14, 17–29, <https://doi.org/10.5194/bg-14-17-2017>,
1824 2017.
1825

1826 Whiticar, M. J.: Carbon and hydrogen isotope systematics of bacterial formation and
1827 oxidation of methane, *Chemical Geology*, 161, 291-314, [https://doi.org/10.1016/S0009-](https://doi.org/10.1016/S0009-2541(99)00092-3)
1828 2541(99)00092-3, 1999

- 1829
1830 Wu, F., Li, J., Peng, Z., Deng, N.: Photochemical formation of hydroxyl radicals catalyzed by
1831 montmorillonite, *Chemosphere*, 72, 407-413,
1832 <https://doi.org/10.1016/j.chemosphere.2008.02.034>, 2008
1833
1834 York, D.: Least squares fitting of a straight line with correlated errors, *Earth and Planetary*
1835 *Science Letters*, 5, 320-324, [https://doi.org/10.1016/S0012-821X\(68\)80059-7](https://doi.org/10.1016/S0012-821X(68)80059-7), 1968
1836
1837 York, D., Evensen, N. M., Martinez, M. L., and De Basabe Delgado, J.: Unified equations for
1838 the slope, intercept, and standard errors of the best straight line, *Am. J. Phys.* 72, 367-375,
1839 <https://doi.org/10.1119/1.1632486>, 2004